Seismic retrofit design and risk assessment of an irregular thermal power plant building

Jianze Wang[a], Kaoshan Dai[b,]*, Bowei Li[c] , Bo Li[b], Yang Liu[b], Zhu Mei[b], Yexian Yin[d], and Jiahong Li[e]

a Department of Disaster Mitigation for Structures, Tongji University, Shanghai, China.

b Department of Civil Engineering and Institute for Disaster Management and Reconstruction, Sichuan University, Chengdu, China;

*Corresponding author's email address: kdai@scu.edu.cn

Key Laboratory of Deep Underground Science and Engineering, Ministry of Education, Sichuan University, Chengdu, China.

c Department of Civil and Environmental Engineering, University of Michigan, Ann Arbor, USA.

d SEPCOIII Electric Power Construction Corporation, 882 Tong'an Rd, Qingdao, China.

e Hongrui Electric Power Engineering Consulting Co., 882 Tong'an Rd, Qingdao, China.

Abstract: Electric power system is one of essential lifeline systems for an urban community. An actual power plan building with typical coal-fired power generation process is selected to be studied in this paper. The detrimental impacts on the seismic performance of the structural system induced by heavy coal bunkers and irregular bracing configurations are expected to be mitigated by using retrofit strategies. A total of three retrofit design schemes which employ the isolation and supplemental damping techniques are developed. The original design scheme of the actual thermal power plant building that adopts steel special concentrically braced frame as lateral-force resisting system is used as benchmark for comparison purposes. Nonlinear response-history analyses are performed, and the obtained seismic responses are compared. To better quantify the benefit of the considered retrofit strategies, seismic risk in terms of probabilities of exceedance for designated damage states as well as the downtime are analyzed. For the studied TPP building, the results show that the added damping system is more effective in seismic risk reduction than the isolation for heavy coal bunkers. Compared to the original structural system design, the use of supplemental damping system cut the downtime of the thermal power plant building at most 42%.

Keywords: Thermal power plant; Industrial building; Retrofit design; Seismic risk; Irregular structure; Isolation; Damper.

1 Introduction

Earthquake, as a destructive natural disaster, needs to be considered into the structural design of industrial plant buildings. The reconnaissance reports for recent seismic events such as Bam earthquake in 2003 [1], Chile earthquake in 2010 [2], Great East Japan earthquake in 2011 [3], Emila earthquake in 2012 [4] pointed out the high vulnerability of industrial plants would cause life threatening, economical losses and environmental contamination after the earthquakes. Seismic damages were observed both in structural and nonstructural components such as column supports, girders, mechanical equipment, piping systems and storage racks. The resulting consequences ranged from the complete collapse to temporarily shut-down, and included a high likelihood of triggering uncontrolled fires and possible environmental damage [5]. Electric power system is an essential part in an urban community. Nowadays, the majority of global electricity generation is using fossil fuels [6]. Coal-fired thermal power plant is one of the most commonly used power plants and providing 40% of the world's electricity, especially in developing countries [7]. The functional interruption of a power plant due to earthquake disasters would result in immense economic and social loss to its associated urban regions.

Currently, common routines for seismic design of industrial buildings still follows conventional building design codes such as ASCE/SEI 7-10 [8] and Eurocode 8 [9]. Similar to residential building structures, the industrial building design is performed with the basic objective of to prevent building collapse under the maximum considered earthquake (MCE). In

39 fact, as the thermal power plant is a part of the urban power generation system, a more stringent objective, which is the

40 continuous operation after moderate and small earthquake, is required. It can be achieved by elevating risk level in

41 structural design and subsequently enlarging seismic demands in mandatory. As such, Chilean Ministry of Housing recently

42 revised the design procedure for industrial buildings (i.e. NCh 2369) [10] with an intention to guarantee the continuous

43 functionality of steel industrial structures even if the earthquake loading is sever than design-based earthquake intensity.

44 However, recent earthquakes (e.g., Chile in 2010; Emila earthquake in 2012) have demonstrated that although buildings

45 that were designed based on conventional seismic provisions endured minimal structural damage by earthquakes, they were

46 still nonoperational because of extensive nonstructural damage [2,4].

47 Nowadays, the performance-based design theory is widely developed and studied with the purpose to provide

48 engineers and stakeholders with informed and quantified descriptions of consequences for decision making. The

49 performance-based design basically entails the integration of seismic hazard, seismic demand estimation, fragility

50 development and loss estimation. Compared to the conventional design methods with limited basic objectives, the

51 performance-based design theory enables practical engineers to set more specific design objectives and evaluate the design

52 results in terms of repair cost, operational downtime and life safety. In the past years, plenty of studies regarding

53 performance-based structural design were performed. For example, Ellingwood [11] proposed a seismic risk assessment

54 framework and applied it to steel and reinforced concrete frames. Rojas *et al*. [12] provided an automated performance-

55 based design methodology to optimize the performance of structural and nonstructural systems of regular steel buildings

56 in terms of social loss. Similarly, Hwang and Lignos [13] estimated the earthquake-induced loss of steel frame buildings

57 by using a building-specific loss estimation methodology developed by Ramirez and Miranda [14]. In addition, the

58 performance-based design theory was applied to innovative structural systems like self-centering moment frame [15] and

59 buildings equipped with damping systems [16,17]. Tafakori *et al.* [18] performed risk-based retrofit design on an existing

60 tall steel building. And eight retrofit alternatives were compared in terms of seismic risk and annual loss. Similarly, cost-

61 benefit analyses were conducted by Liel and Deierlein [19] with the purpose to assess retrofit strategies on non-ductile

62 concrete frames. Han *et al*.[20] studied the benefit of using isolation technique on nonductile concrete buildings against

63 the economic cost and indirect losses due to downtime and fatalities were also considered.It is worth noting that most

64 previous studies focused on civil constructions and few studies extended the use of performance-based design method to

65 industrial buildings.

66 Since lessons from past earthquake events confirmed the devastating impact on industrial facilities, in order to

67 improve the seismic resilience and prevent consequent accidents, some researchers applied seismic mitigation strategies to

68 the industrial buildings. For example, Colombo and Almazán [21] assessed the influence of energy dissipation systems on

69 the seismic damage of cylindrical steel tanks. Kanyilmaz and Castiglioni [22] performed incremental dynamic analyses to

70 assess the merits of base isolations in industrial steel silos. The simulation results showed that the base isolations reduced

71 the story drift demands as well as the collapse risk under strong earthquakes. Similarly, Rossi *et al*. [5] introduced friction

72 pendulum isolators at the top of columns of supporting silos and they found that the use of isolations eliminated the torsional

73 effect and protected steel braces from buckling. In addition, a torsional hysteretic damping device was used into the retrofit

74 design of existing silo structures in studies by Pinkawa *et al.* [23]. The conducted incremental dynamic analysis results

75 showed its effectiveness in preventing the global side-way collapse failure mode. Paolacci *et al*. [24] compared the

76 efficiency of base isolation, energy dissipation devices and traditional tuned-mass-damper device in seismic response

77 reduction for chemical process plants by means of numerical simulations and physical tests. Noted that, most prior studies

78 discussed the performance of seismic mitigation strategies in the aspect of structural behaviors and few built a link with

79   the seismic risk.

80   In this study, an actual thermal power plant (TPP) building is considered. The seismic risk of the TPP building and

81   the effectiveness of different seismic mitigation technologies in reducing the seismic risk are studied. At first, the

82   performance-based retrofit design of the TPP building is performed. Unlike common residential buildings, the challenge

83   of the design work is not only to properly communicate with the operational process but also consider how to protect the

84   industrial equipments under earthquake loadings. One of the critical equipment, i.e. coal bunkers, is accounted into the

85   lateral-force resisting system (LRFS) design of the TPP building. Subsequently, based on the complex structural topology

86   of the building, the feasibility of the considered retrofit techniques in the TPP building is discussed. Following the modern

87   building design provisions, a conventional LRFS system design and three retrofit system designs are developed. Nonlinear

88   response-history analyses are conducted and afterwards, seismic risks of all designed buildings are computed and

89   compared. The effectiveness of the selected retrofit techniques is discussed. Finally, the contributions and limitations of

90   the study are provided, followed by the conclusion section.

2   A typical thermal power plant building

2.1   Functional classification and structural configurations

93   In TPPs, the electric power is generated mainly by steam-driven turbines. In general, the power generation process includes

94   several interconnected sub-systems like steam and power generation system, coal conveyor system, coal crushing system

95   and feedwater system. The associated equipment and processing units of these sub-systems are mostly placed in a single

96   industrial building which lead to the great importance of the building to the whole power plant. The typical configuration

97   of the TPP building can be seen in in Fig.1. Based on the power generation process and equipment arrangement, the TPP

98   building can be mainly divided into three parts: turbine hall, deaerator bay, and bunker bay.
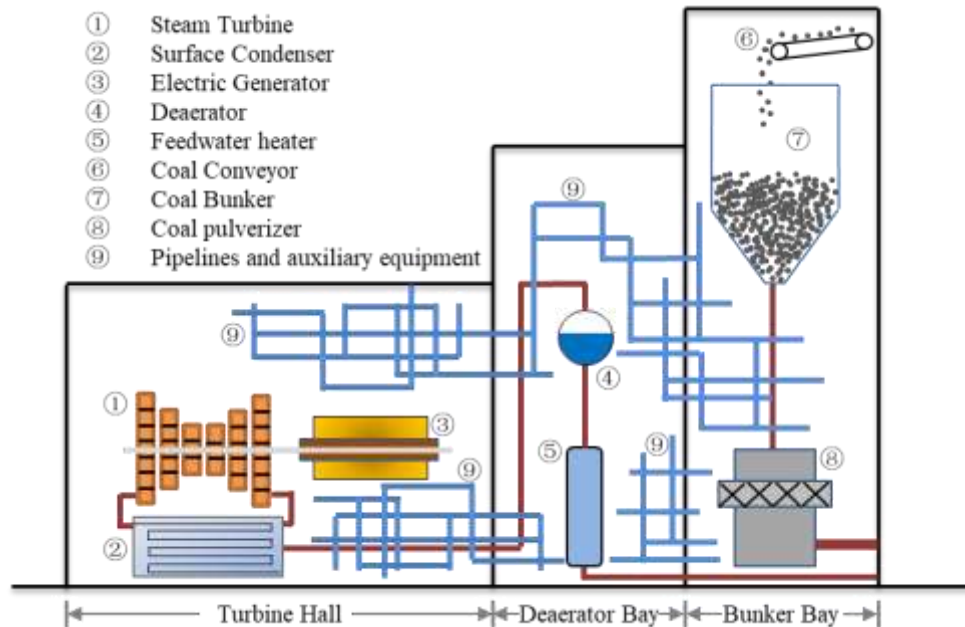

99

100   **Fig. 1.** Facility and equipment arrangement in the main industrial building of a typical power plant

101   The complex operational process raises plenty of constraints and limitations to structural design and consequently

102   results in an irregular configuration for the TPP building. The structural typology of an actual TPP building considered in

103   the current study can be seen in Fig.2. The building is generally 54.1 m × 92 m in plan at the base. The spacing of frames

104   along X direction is 10 m. The spans of turbine hall, deaerator bay, and bunker bay are 30.6 m, 10 m, and 13.5 m; the

105   corresponding heights are 30.5 m, 38.4 m, and 53.3 m, respectively. The building also includes an extension at the north-

106   east corner of the bunker bay (between Axis-01 and Axis-1) with a 6m-tall penthouse at the top. The lateral-force resisting

107   system (LFRS) adopts concentrically braced frame and the distribution of braced frames is indicated in Fig.2a. Also,

108   Figs.2b and 2c show the elevation views of the structure along X and Y direction, respectively. Each axis in X direction

109   (i.e. Axis-A, B, C, D) has two braced frames that are between Axis-1 and Axis-2 and between Axis-9 and Axis-10. In

110   contrast, it is noted that the operational process generates larger impact on the frame configuration in Y direction.

111   Specifically, as seen from Fig.2b, the turbine hall is configured as a high-clearance warehouse and the deaerator bay is

112   designed as high-story moment frames so as to provide enough extension spaces for piping systems (Fig.1). The bunker

113   bay is configured with chevron and inverted-chevron braces. With the intension of large-caliber pipelines and equipment

114   freely cross the building, the 1st-tier braced frame in bunker bay is designed with a "half" inverted-V type bracing. More

115   specifically, there is only one brace member that connects the column base of Axis-D to the middle of the girder on the 1st-

116   tier floor. Similarly, for the roof tier, a moment frame is used to resist lateral loadings instead. Another issue is worth noting

117   in the structural design of the TPP building is that there are 7 coal bunkers shaped like silos installed at the 32.2 m level of

118   the bunker bay. The coal bunkers are a vital part of the supply chain and their loss of functionality may lead to business

119   disruption of the whole TPP. For a common practice, the coal bunkers are rigidly connected to the girders by using 12-

120   fixed supports. An illustration of the coal bunkers in the structural building can be seen in Fig.3. The seismic mass of each

121   coal bunker which is the sum of the weight of an empty bunker and the coal materials under normal service conditions is

122   as much as 1040 tons. Therefore, in seismic design especially for the structural part in bunker bay, a total of 7280 (7×1040)

123   tons of mass at the 32.2 m level shall be considered. Such large mass concentration would impose detrimental effects on

124   the seismic performance of the structure [25].

125
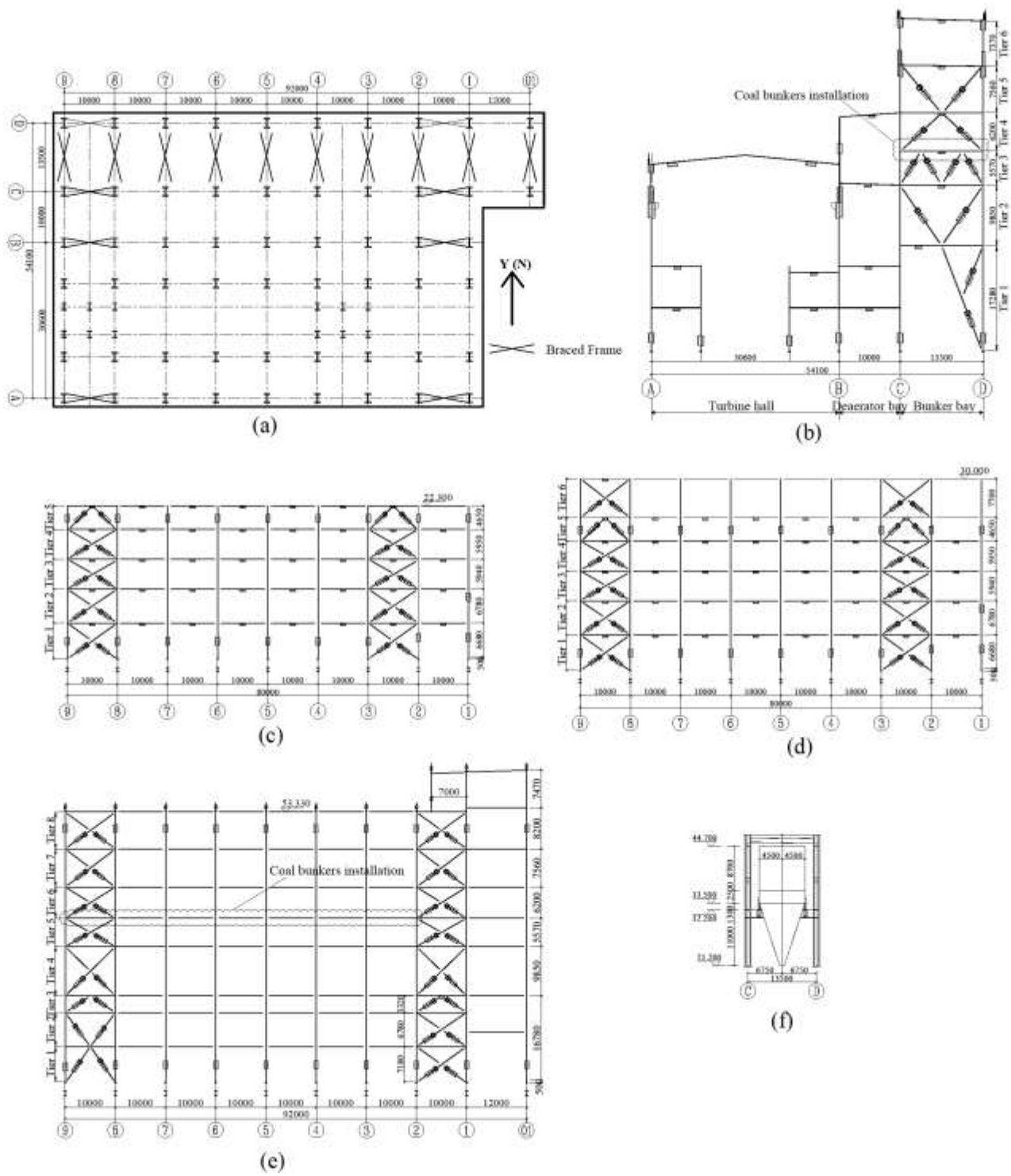
Fig. 2. A typical TPP building considered in the study: (a) Plan layout at the base, (b) Elevation view along Axis-5, (c) Elevation view along Axis-A, (d) Elevation view along Axis-B, and (e) Elevation view along Axis-C/D (f) Elevation view of a single coal bunker.

2.2 Resilient strategies for retrofit design of the TPP building

The resilience of a building structure can be enhanced by using isolation techniques, supplemental damping systems, or a combination of these [18,26,27]. By strategically using these techniques, structural repair and/or replacement of the added

132   devices in the aftermath of an earthquake can be done in a short time. For the TPP building, suitable resilient strategies
133   need to be selected to compromise with the corresponding structural topology and operational constraints. Specifically, the
134   large concentrated seismic mass (due to the existence of coal bunkers) and potential weak stories (due to discontinuous
135   bracing systems) are of key interest to the retrofit design. Also, the damping system design (i.e. collections of damping
136   devices and associated structural elements used to transfer forces from damping devices to LFRS [8]) is not allowed to
137   interfere with the normal operational process. In other words, the supplemental damping systems are only permitted to be
138   placed where the braced frames in the original structural system as shown in Fig.2a. Such constraint requires the damping
139   system is capable to provide initial lateral stiffness and energy dissipations for a purpose to avoid soft/weak stories due to
140   sudden changes in lateral story stiffness/strength. Hence, metallic yield damping devices are preferred to be employed.

141   As indicated in prior studies, a significant contributor to total loss in special concentrically braced frame (SCBF)
142   building systems is the repair cost for bracing components [28]. In addition, flexural buckling of steel braces typically
143   occurs at a story ratio of approximately 0.5% in average which may result in discontinuous operation of the TPP building
144   under moderate earthquake loadings. Instead of the conventional hollow or wide-flange sectional bracing elements,
145   buckling restrained braces (BRB) are firstly considered as an alternative because of their stable and consistent hysteretic
146   behaviors in both tension and compression [29]. Another device considered in the retrofit design of the TPP building is the
147   yielding shear panel device (YSPD), which dissipates energy by inelastic shear deformation of a low-yielding-point steel
148   plate. As tested by previous studies, it has been demonstrated that the YSPD has a sound energy dissipation capacity and
149   adequate elastic stiffness to withstand in-service lateral loadings (e.g. wind) [30].

150   As for the heavy coal bunkers installed at the level of 32.2 m, retrofit strategies are needed to reduce their adverse
151   impact on the seismic demands of their supporting structural components. From past earthquake reconnaissance reports,
152   similar storage silo-shaped facilities that commonly used in industrial structures caused severe damage even collapse to
153   the supporting structural system [31]. Therefore, some researchers employed base isolations as a retrofit solution for
154   existing industrial silo-type structures with an attempt to improve their seismic performance (e.g. [23,32]). As such, for the
155   TPP building that are characterized by heavy coal bunkers, Dai *et al*. [33] introduced a partial mass isolation system and
156   proposed a probabilistic-based design framework. The effectiveness of the isolation layers is optimized in terms of story-
157   drift reduction with respect to a non-isolated structural system. In the following retrofit design for the TPP building, the
158   isolation strategy is also considered specific for coal bunkers and the associated isolator properties are determined using
159   the method proposed by Dai *et al*. [33].

160   In sum, two resilient retrofit techniques – added damping system which includes YSPD and BRB as well as isolation
161   technique for coal bunkers are considered in this study. A total of three retrofit design schemes are developed including (1)
162   Retrofit Design-A: use of isolation system for coal bunkers; (2) Retrofit Design-B: use of supplemental damping systems
163   in LFRS design; (3) Retrofit Design-C: combined use of isolation and supplemental damping systems. The original
164   structural system design is used as the baseline to compare against the three developed resilient structural systems.

3   Structural retrofit designs

166 The actual TPP building was originally designed according to the modern design codes AISC 360-10 [34], AISC 341-10
167 [35] and ASCE/SEI 7-10 [8]. The design loads primarily include dead load, live load, wind load and seismic load. The
168 associated load combinations were performed in accordance with ASCE/SEI 7-10 standard. As shown in Fig.2, braced
169 frames are placed in LRFS of both principal structural axes. The design requirements related to SCBF system prescribed
170 in AISC 341-10 are followed. The wide flange sections are adopted for columns and beams. The square hollow structural
171 shapes (HSS) are used for brace members. The beam-column connections are welded so fully restrained assumption is

172   made in design analyses. The braces are connected to columns and beams through gusset plate connections and each has

173   an elliptical clearance of eight times the thickness of the gusset plate so as to accommodate brace-end rotation demands

174   [36]. The strength (e.g. compression, flexure, buckling) of every structural component as well as connections are examined

175   in accordance with AISC 360-10 [34]. The TPP building is actually located at a high seismic-prone zone in China with Site

176   Class D. The corresponding mapped spectral acceleration parameters, i.e. S_s at short period and S_1 at a period of 1s, are 1.4

177   g and 0.9 g, respectively. As the TPP building is constructed as a kind of lifeline facilities, the Risk Category of III and

178   Seismic Design Category D are assigned. And hence, the importance factor $I = 1.25$, response modification factor $R = 6$,

179   deflection amplification factor $C_d = 5.5$, and overstrength factor $\Omega_0 = 2.0$ are considered in the original design of the LRFS

180   for the TPP building.

3.1 Retrofit Design-A: Isolation system for coal bunkers

182   The first retrofit design only employed isolation technique specific for the heavy coal bunkers at the level of 32.2m of the

183   frame between Axis-C and Axis-D (i.e. bunker bay). Again, for a conventional practice, the coal bunker is rigidly connected

184   to the girders by using 12 fixed-supports. With the introduction of isolation strategy, the fixed-supports are replaced by

185   lead-rubber bearing (LRB) isolator devices and an illustration can be seen in Fig. 3. The isolation layer which is composed

186   of 12 isolator devices for each coal bunker is fabricated with a purpose to reduce the inertial motions of the heavy coal

187   bunkers. The compression strength of the LRB isolator is ensured to have the ability to withstand the vertical loadings

188   imparted by the connected coal bunker. The initial stiffness of the isolation layer is designed to be large enough to resist

189   the serviceable loads such as wind loadings and lateral impact by falling of coal materials from the top conveyor. The

190   effective stiffness of the isolator device is a key property to the performance of the entire isolation system. The idealized

191   situation is where the movement mechanism of the isolated coal bunker is designed to work as a tuned mass damper.

192   Therefore, the lower supporting structures are subjected to the anti-motion force induced by the coal bunkers. Such design

193   was achieved in another study of the authors' [33]. The installation space in-situ and allowable deformation should also be

194   considered in the sizing of the isolator device. An isolator device available in business market is used and the corresponding

195   parameters are listed in Table 1. The allowable deformation of the isolation device is limited by the gap of two adjacent

196   coal bunkers (i.e. 400 mm as seen in Fig.3) in case of pounding during an earthquake, also limited by the deformation

197   capacity of the isolator (i.e. 385 mm). Based on the stiffness properties of the selected isolator and the seismic weight of a

198   coal bunker, the natural period of a single isolated coal bunker is computed as 2.11s.
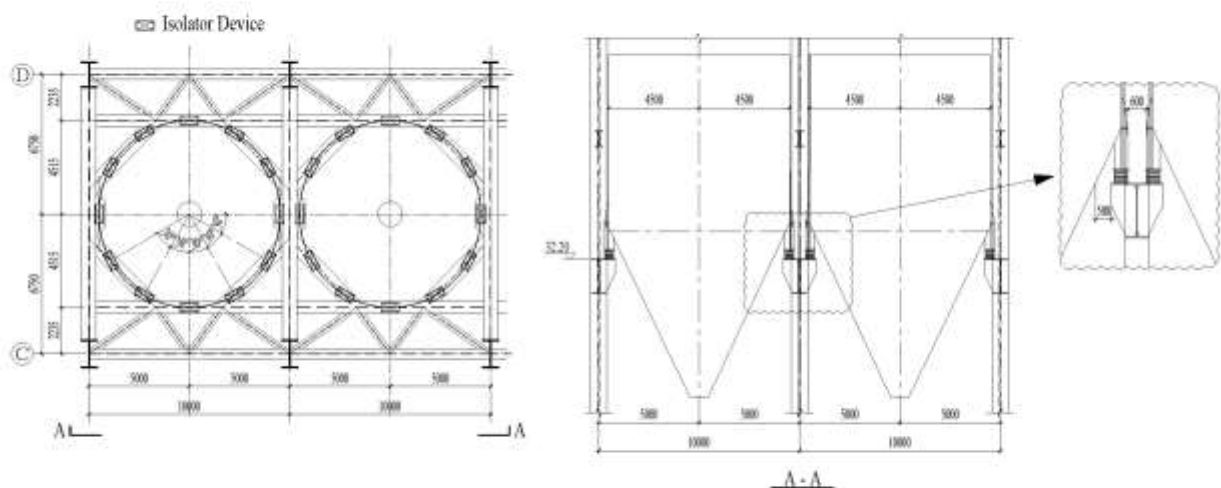
199

200   **Fig. 3.** Schematic illustration of coal bunker isolation

3.2 Retrofit Design-B: Use of damping system in LRFS design

201

202 As discussed in Section 2.2, the YSPD and BRB devices are considered in the retrofit design. The Chapter 18 of ASCE/SEI

203 7-10 that details the requirements of structural design with added damping systems is followed. A value of 8% additional

204 effective damping to the LRFS in each principle direction of the structure is set as the design objective. Although there

205 have been proposed design methods for structures with supplemental dampers in prior studies, an iterative process for

206 design objective achievement is inevitable [37]. Based on the original design scheme, an iterative design work that include

207 variations in properties of damping devices as well as their distribution is carried out with the help of SAP2000 V18 [38].

208 The locations, numbers and properties of damping systems are presented in Table 2. The initial stiffness of BRB device

209 stands for the elastic stiffness of the steel yielding core which is later used in the numerical modeling. The initial stiffness

210 of YSPD is the average tangential stiffness of the steel plate before yielding and the value of which is usually provided by

211 the manufacture. The bracing elements that transfer forces from YSPD to the rest seismic structural members are designed

212 to remain elastic under earthquake loadings in MCE intensity. The inverted V-configured and X-configured bracing systems

213 are used for the YSPD connection (Fig. 4a).

214   It is also noted that the bracing system at the top two tiers of the Y-directional frames (Fig.2b) is discontinuous which

215 may lead to weak and soft tiers. The coal conveyor which is located at the 6th-tier in the bunker bay (Fig.1) has to extent

216 through the building along X direction (i.e. from Axis-01 to Axis-9). It is a part of the supply chain for coal material in the

217 TPP building and therefore, the structural damage in the 6th-tier is expected to be reduced. However, supplemental damping

218 systems such as diagonal BRB and YSPD together with V-type or X-type bracings are not allowed due to their architectural

219 obstructions. Instead, the moment frame of 6th-tier in the bunker bay is strengthened by using stocky knee braces, as

220 presented in Fig.4b. The effectiveness of the knee-braced system has been investigated [39–41] by means of physical tests

221 and numerical analyses. Using the design method provided by Leelataviwat *et al.* [42], yielding and buckling damage

222 initially occurs at the knee braces and then followed by plastic hinging formation in the connected moment frame. The

223 damaged knee brace can be repaired and/or replaced after an earthquake which helps to facilitate the functional recovery

224 and structural repair process.

225
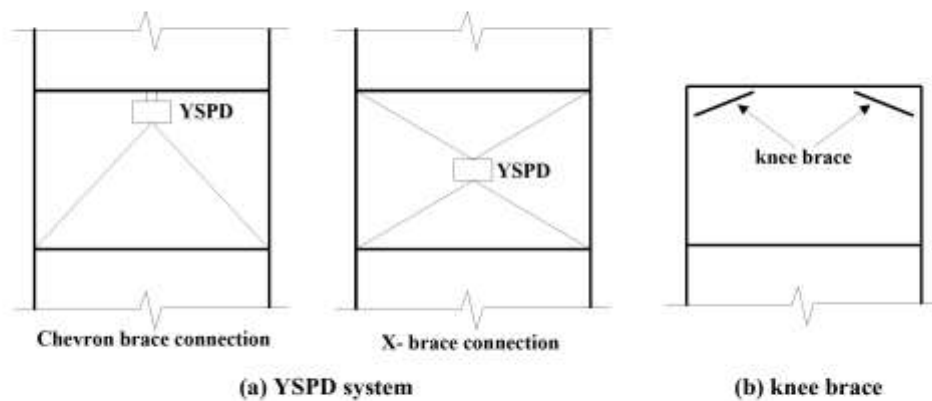
226 **Fig. 4.** Schematic illustration of utilized resilient strategies

3.3 Retrofit Design-C: Combined use of isolation and supplemental damping system

227

228 For the Retrofit Design-C, both techniques of the isolation for coal bunkers and supplemental damping systems are utilized.

229 Since the heavy coal bunkers are installed on the level of 32.2m in bunker bay, the considered isolation strategy is likely

230 to benefit the substructures below the coal bunkers only (i.e.1st to 5th tiers for Axis-C&D and 1st to 3rd tiers for Axis-1 to 9

231 (Fig. 2)). For the rest substructures (i.e. frames between Axis-A to Axis-B and frames above coal bunkers between Axis-C

232   to Axis-D), the damping devices are added to reduce the corresponding seismic demands and structural damage.

233   With a comparison purpose, the properties of isolator devices for Retrofit Design-C adopted those same with Retrofit

234   Design-A (Table 1). Considering the use of isolation for coal bunkers, the supplemental damping system is mandatorily

235   prohibited for the structures below the coal bunkers which are specifically the frames between Axis-C and Axis-D. On the

236   contrary, for frames in Y-direction (i.e. Axis-1 to Axis-9), BRB devices are still considered for the 1st-tier due to the

237   unsymmetrical bracing configuration (Fig.4d). Analogous to the Retrofit Design-B, the added damping systems are

238   designed following the Chapter 18 of ASCE/SEI 7-10 and the design results are listed in Table 3. The knee-brace strategy

239   is also employed for the roof tier in Y-directional frames.

4   Numerical Modeling

241   Recall that the original TPP building design as well as the three retrofit designs were examined using SAP2000 V18. The

242   first three mode shapes of the original TPP building are presented in Fig. 5. The first two modes follow translational motions

243   patterns along the two principle directions of the building. And the third mode follows torsional motion around the vertical

244   axis of the building. It is noted that due to the complex structural configuration of the TPP building, the effective mass

245   ratios of the 1st and 2nd translational modes are as much as 63% and 73%, respectively. And hence, a total of 60 modes were

246   considered in dynamic analyses so that the accumulated modal mass participated in translational motions in each principle

247   axis of the building is greater than 90%. The mode periods of the original design and three retrofit designs are compared

248   in Table 4. It can be seen from the table that the dynamic properties of the four designed buildings are close. The obtained

249   dynamic characteristics are also similar to the study result provided by Dai *et al*. [33], which verifies the sufficiency of the

250   developed numerical model.

251   Three-dimensional nonlinear structural models for all considered building designs are built using PERFORM-3D [43]

252   which enables the nonlinear response history analyses (RHAs) conducted with a sound efficiency and convergence. Every

253   numerical model includes both the LRFS (i.e. braced frames) and the gravity framing system. The Rayleigh damping of

254   3% at $0.2T_1$ and $1.0T_1$, where T_1 is the fundamental period, is considered in RHAs. Also, a time step of 0.005s is assigned

255   to each loading case. Global P-Δ effect is directly incorporated in the analysis and geometric nonlinearity is assigned to all

256   structural elements. The nonlinear dynamic analyses are set to terminate when the solution fails to converge or when

257   excessive roof drift ratio of 10% in the principal structural axes is reached. A 10-s duration of zero-amplitude acceleration

258   time history is added at the end of each ground motion to identify the residual drift after the actual excitations.

259   The modeling techniques for structural components, isolators, and damping systems are verified and presented in
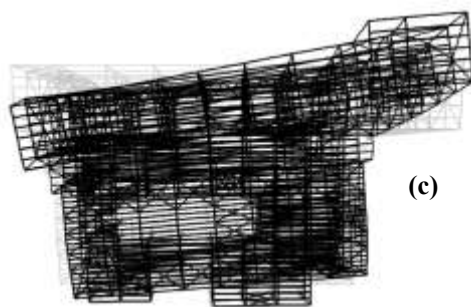
260   detail in the following sections.

261

(c)

262
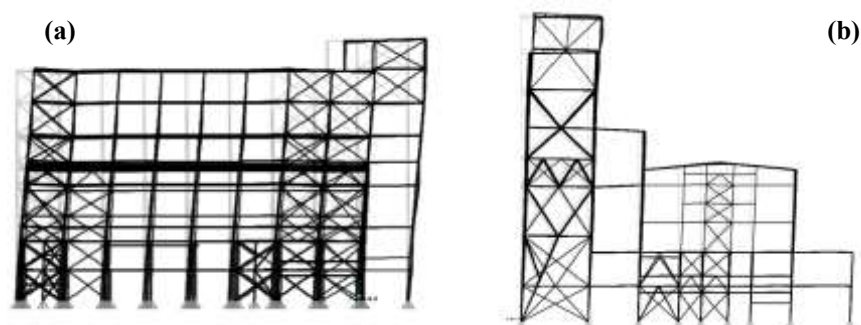
263 **Fig. 5.** Mode shapes: (a) Mode 1 – translational motion along X dir.; (b) Mode 2 – translational motion along Ydir.; (c)

264 Mode 3 – Torsional motion

265 **4.1 Braced frame**

266 As prescribed by AISC 341-10 [35], columns and beams in SCBF are designed as force-controlled components and braces

267 are designed as deformation-controlled components. In other words, columns and beams shall remain essentially elastic

268 even under severe earthquake loading. Braces are expected to behave nonlinearly to dissipate energy. The potentiality of

269 going into plastic for beams and columns are still considered in numerical model, by assigning flexural nonlinear hinges at

270 both ends of components. The backbone curve of the nonlinear hinge elements provided by PERFORM-3D [43] can be

271 seen in Fig.6a. The required parameters such as F_Y, F_R, a, b are determined based on suggestions from ASCE/SEI 41-13

272 [44].

273 The buckling behaviors of braces is simulated by using the nonlinear steel bar/tie/strut element wrapped with buckling

274 materials. Such nonlinear model follows an elastic perfectly-plastic backbone in tension and a buckling relationship in

275 compression. The corresponding backbone curve can be seen in Fig.6b. The stress values specified for point A and point B

276 are assigned with 1% and 15% of tension strength, and the strain values are 45% and 50% of the strain range of the

277 hysteresis loop, respectively. The stretch factor, which controls the tension stretch after an increased buckling deformation,

278 is taken as the value of 0.75. The ductility ratio and residual strength (after strength deterioration) for braces in tension and

279 in compression are obtained from stipulations in ASCE/SEI 41-13 [44]. The parameter values mentioned above are verified

280 by using the results from cyclic loading tests of a single-bay braced frame [45]. Fig.7 shows the comparison between the

281 simulation and test results on the hysteretic loops of a brace element. A good agreement in the aspects of yielding/buckling

282 strength and deteriorations in strength and stiffness is achieved as seen from the figure.
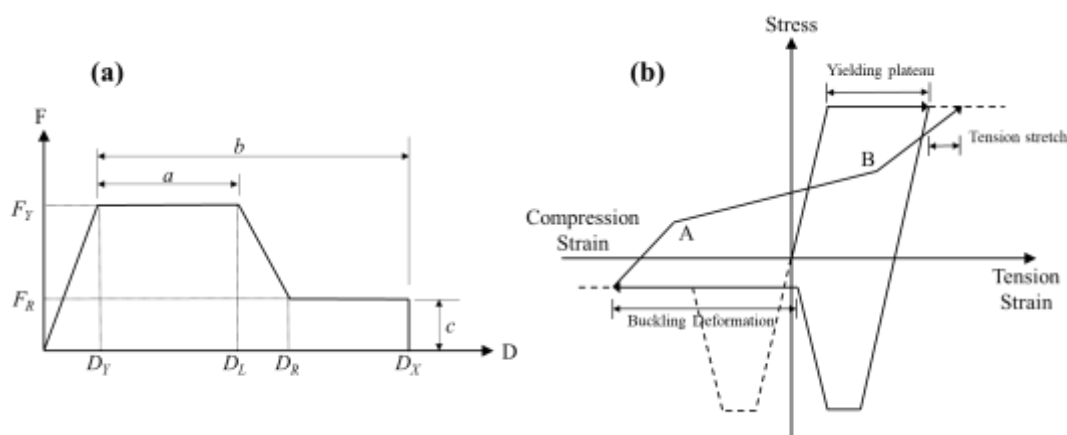
283

284

285 **Fig. 6.** Finite element models used for braced frame components: (a) backbone curve for nonlinear hinges; (b) hysteric
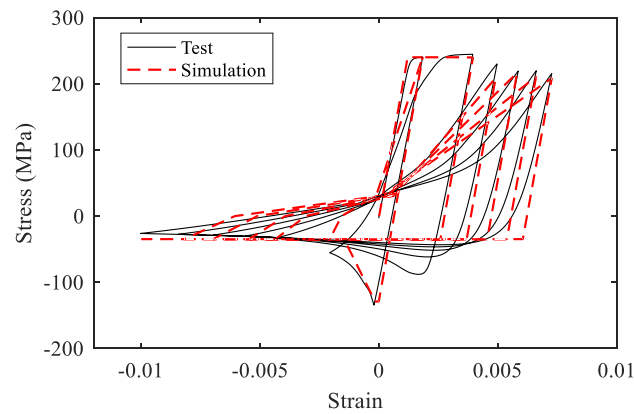
286 model for brace elements[43]

287

289   **Fig. 7.** Comparison of hysteretic behaviors of brace element between test result and numerical simulation

290   **4.2 Isolations for coal bunkers**

291   The simulation of coal bunker was simplified by using body-constrained nodes which include supporter nodes and a mass

292   node located at the center of gravity of the entire coal bunker. A schematic view of the simplified model can be seen in

293   Fig.8. The center of mass node (blue point in Fig.8) is assigned with the seismic mass of an entire coal bunker (i.e. 1040

294   tons). The effectiveness of such simplified model for coal bunker was also studied by Pinkawa *et al*. [23]. In this study, the

295   fixed supporters for coal bunkers in the Original Design and Retrofit Design-B are modeled using rigid links. For Retrofit

296   Design-A and Retrofit Design-C (i.e. using isolations for coal bunkers), the isolator device is modeled by rubber-type

297   seismic isolator element available in PERFORM-3D. The hysteric behavior of such element is basically described with a

298   trilinear model (Fig.9a). The initial stiffness K_0, post-yielding stiffness K_F, yielding strength F_Y, allowable deformation D_X

299   are specified according to Table 2. Oher parameters required in the model, specifically F_U and D_U, are taken as 1.25 times

300   the yielding strength and 3.75 times the yielding deformation, respectively. The parameter values as taken above are also

301   verified based on a cyclic loading test result performed on a lead-rubber bearing device [46]. Fig.9b shows the comparison

302   between the test and simulation result of an isolator device and a good agreement is indicated from the figure.

303
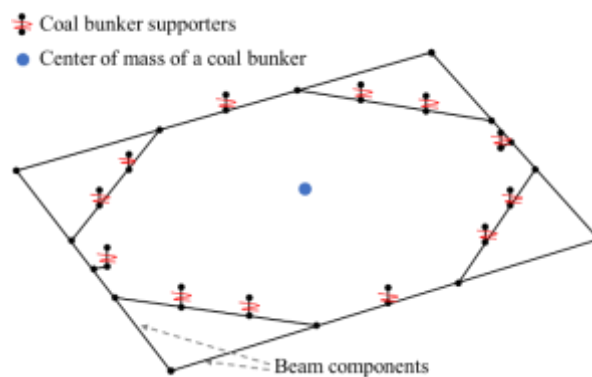
304
305   **Fig. 8.** Schematic view of coal bunker model
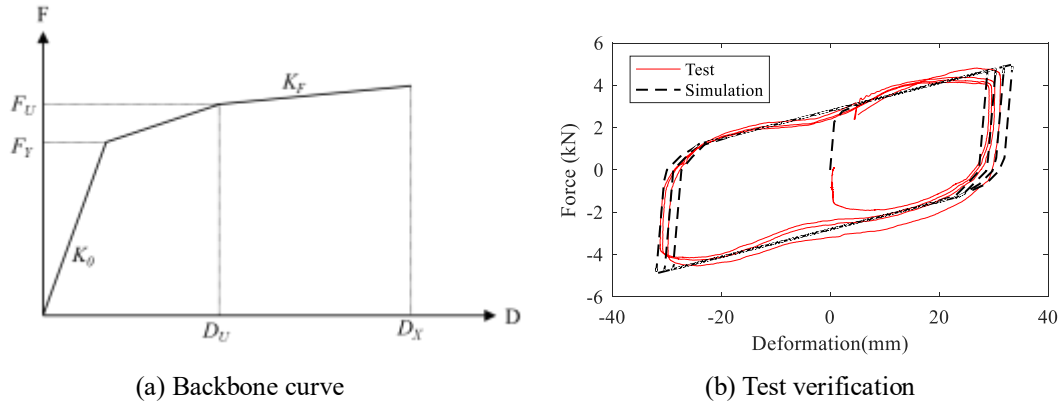
| (a) Backbone curve | (b) Test verification |

Fig. 9. Element model for isolator device

4.3 Modeling of YSPD device

The YSPD device was modeled using the shear-type infill panel element provided by PERFORM-3D [43] which follows a trilinear force-deformation relationship as seen in Fig.10a. The parameters of initial stiffness K_0 and yielding strength F_Y are determined based on Table 2 and Table 3 for Retrofit Design-B and Retrofit Design-C, respectively. The post-yielding stiffness K_H is taken as 18% of K_0. The ultimate strength F_U and deformation D_U are assigned with $1.17F_Y$ and $4.5D_Y$, respectively. The allowable deformation D_X is taken as 10% height of the story where the YSPD is placed. The element model as well as the parameter values are verified by using a cyclic loading test result [46]. The comparison between the test and simulation results is made in Fig.10b and it shows that the considered element model is adequate to predict the hysteretic behaviors of the YSPD device.

| (a) Backbone curve | (b) Test verification |
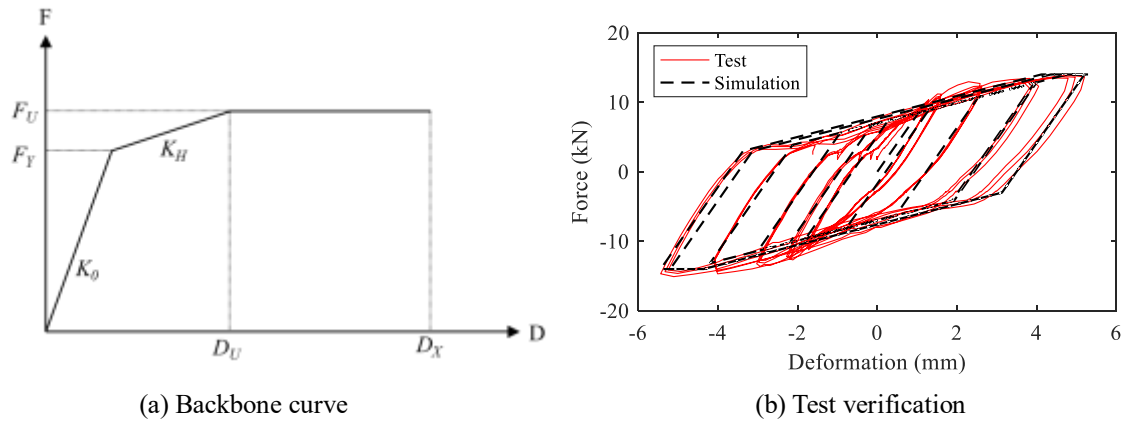
Fig. 10. Element model for YSPD device

4.4 Modeling of BRB component

PERFORM-3D [43] provides a specific element for modeling BRB component and the corresponding force-deformation relationship is shown in Fig.11a. The yielding strength and elastic stiffness of BRB components considered in the Retrofit Design-B and Retrofit Design-C are determined by the values indicated in Tables 2 and 3, respectively. The upper bilinear lines beyond F_Y point in the model is to account for isotropic hardening effect which induces increase in the component strength under cyclic loadings. In this study, the amount of strength increase is considered by selecting "maximum deformation only" in PERFORM-3D and specifying 2.0 for maximum deformation at F_{U0} - F_{UH}, 3.5 for maximum deformation at F_{UH} as suggested by Speicher and Harris [47]. In addition, the values of $1.11F_Y$ and $1.67F_Y$ are considered for post-yield strength F_{U0} and F_{UH}, respectively. The parameter of deformation D_U corresponding to F_{U0} is taken as the 0.175% of the BRB component length. The value of $1.5\%K_0$ is specified for the post-yield stiffness K_F. And the maximum

331   deformation D_X is determined by 6% of the BRB component length. Such modeling techniques and values of parameters

332   are also verified based on test results performed on a BRB device under cyclic loadings [46]. Fig.11b compares the test

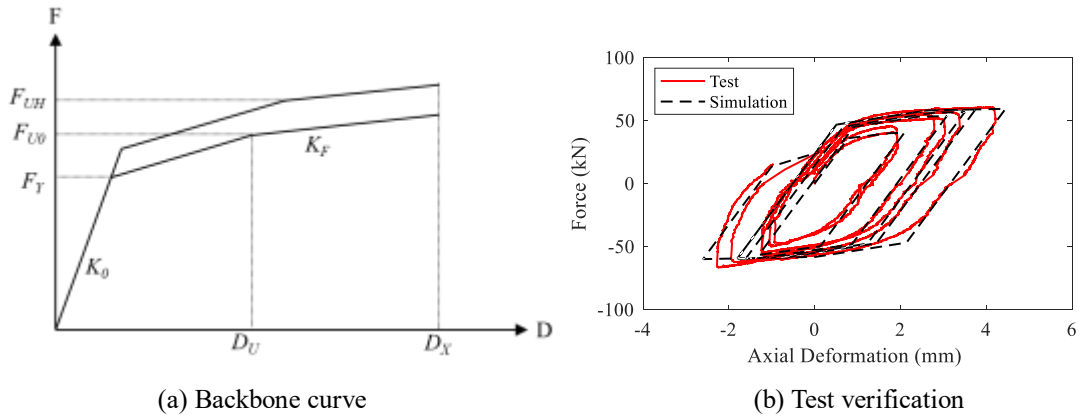333   and simulation results and a good agreement validates the BRB element model as used in this study.

| (a) Backbone curve | (b) Test verification |

Fig. 11. Element model for BRB device

5   Seismic risk analysis

5.1 Ground motion selection

The seismic performance assessment of the developed four design schemes of the TPP building incorporates nonlinear response-history analyses. An ensemble of 15 pair ground motions is selected from PEER NGA database [48] based on the acceleration response spectrum at the MCE intensity (i.e. with an exceedance probability of 2% in 50 years). The spectra of the selected ground motions at the SRSS ordinate as well as the target spectrum are plotted in Fig. 12. The ground motions were selected with the criteria which include moment magnitude (M_w) covers the range of 5.9 – 7.6; the source-to-site distance (R_{rup}) is within 22 – 198.1 km; the average shear velocity in 30 m upper soils ranges from 179 to 276 m/s. The ground motion scaling was done until the median spectrum has a less than 10% mean-square-error with respect to the target spectrum. The details of the selected ground motion are summarized in Table 5. To develop the seismic fragilities, nonlinear response-history analyses are performed at ground motion intensity levels ranging from 60% to 140% of MCE at 20% increment. Such range of ground motions covers the design-based earthquake (i.e. 67% of MCE), the 100% MCE and the extremely rare earthquake incidents (i.e. greater than 100% of MCE). A total of 75 analyses are performed for each designed building.
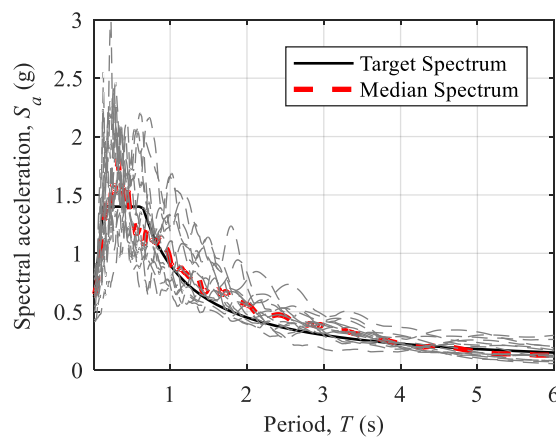
351

Fig. 12. Spectra of selected ground motions and the target spectrum

5.2 Seismic demand comparison

355 The seismic demands of the four considered designed structures are obtained from nonlinear response-history analyses.
356 Fig. 13 compares the roof drift time-history responses of all designed buildings under the ground motion recorded by Delta
357 Station in Imperial Valley earthquake. There it is clear from the figure that the Original Design has the largest value of peak
358 roof drift in X direction (i.e. 0.47%) which is nearly 2 times the values observed from the Retrofit Design-A and Retrofit
359 Design-C. The Retrofit Design-B has the peak roof drift of 0.28% in X direction which is slightly larger than the other two
360 retrofit designs. As for peak roof drift response in Y direction, the considered four building designs have close results. But
361 during the time of 20 to 40 seconds, the Original Design shows the largest response and followed by Retrofit Design-A. In
362 addition, the response histories of the Retrofit Design-B and Retrofit Design-C are almost the same. Noted that the
363 comparison made in Fig. 13 is the results under a single ground motion pair. A total of 75 analysis results for each designed
364 building are statistically processed and discussed in the following.

365

366
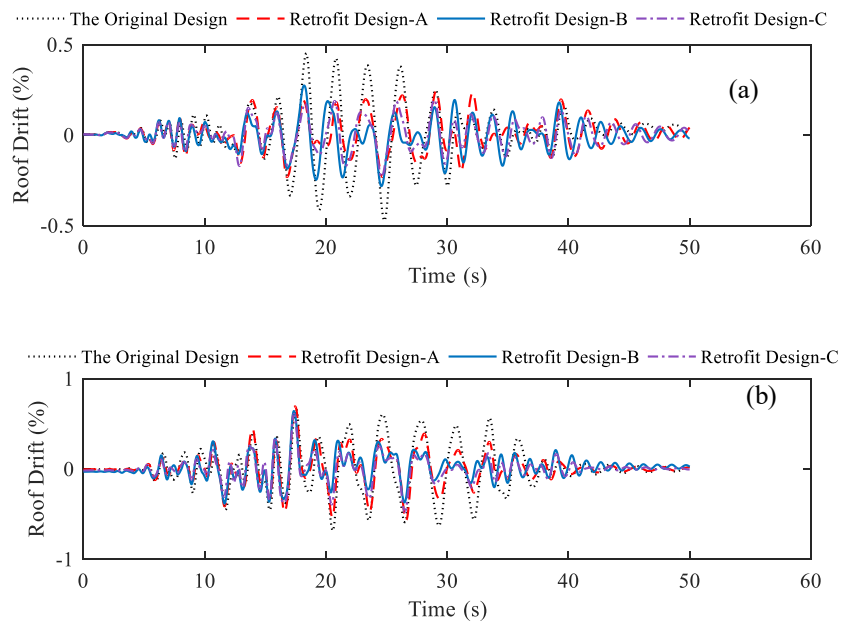
Fig. 13. Comparison of roof drift time-history response: (a) X direction; (b) Y direction

369 **Fig. 14**Fig. 15 show the distributions of peak tier drift ratios under 100%-MCE excitations at the Axis-A, Axis-B and
370 Axis-D frame columns in X-direction and Y-direction, respectively. For drift demands in X-direction, the results of these
371 four are close in some tiers such as the first two tiers in these three axis columns as well as the top tier in Axis-D. For most
372 of the rest tiers, Retrofit Design-B has the smallest drift ratios. On the contrary, the Original Design has the largest drift
373 ratios. The largest difference is observed for results of the 5th-tier in Axis-D where the coal bunkers are installed. The
374 corresponding mean tier drift ratio at the 5th tier of the Original Design is greater than 2%. With the introduction of different
375 retrofit strategies, the drift ratios for Retrofit Design-A, Retrofit Design-B and Retrofit Design-C are reduced to 1.54%,
376 1.10% and 1.34%, respectively. As can be seen from Fig. 15, all the four structures experienced smaller drift demands in
377 Y-direction than those in X-direction. The largest drift in Y-direction is occurred at the 1st-tier for every considered structure.
378 The Original Design has the largest drift ratios at the 1st tier for both Axis-A and Axis-B frames, which are around 1.5%.
379 Conversely, the Retrofit Design-C has the best performance in Y-directional drift response, followed by the Retrofit Design-
380 B and Retrofit Design-A. Taking the results of Axis-A frame as an example, compared to the Original Design, the drifts of
381 the 1st tier are reduced by 15%, 24%, and 33% for Retrofit Design-A, Retrofit Design-B, and Retrofit Design-C,

respectively. In general, it is clear from Figs.14 and 15 that the isolation of coal bunkers (i.e. Retrofit Design-B) did reduce the drift demands not only in tiers that below the coal bunkers in Axis-D frames, but also in tiers of Axis-A and Axis-B frames which are away from the bunker bay (Fig.2). Since the damping systems were uniformly added in Retrofit Design-B, the reduction can be observed in both X-directional and Y-directional drift demands for most tiers. Recall that Retrofit Design-C adopted isolations for coal bunkers along with added damping devices but less than those in Retrofit Design-B. Its performance is in the middle of the other two retrofit designs in terms of the X-directional drift demands and the best in terms of the Y-directional drift demands.
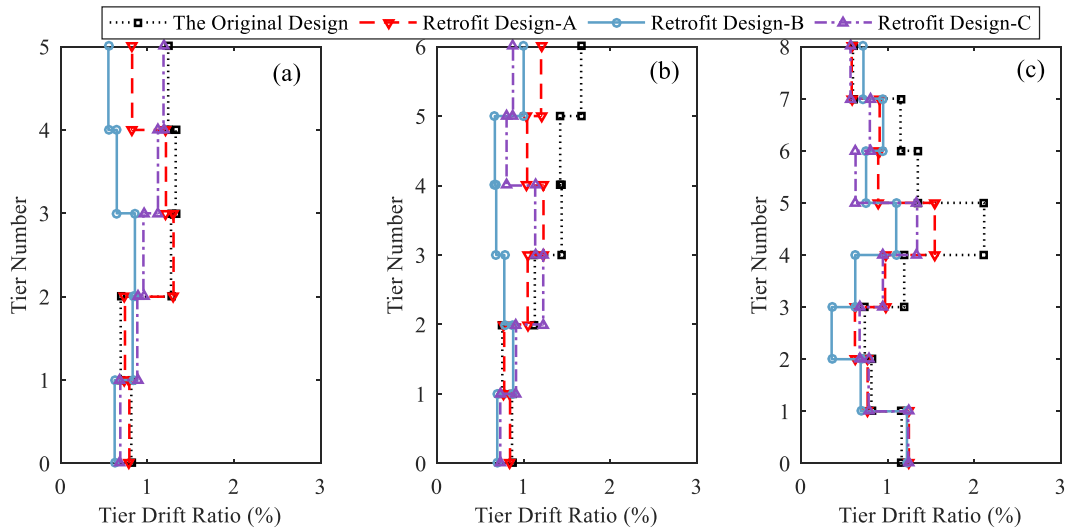
Fig. 14. Distributions of mean story drift ratios under 100%-MCE in X-direction for columns in (a) Axis-A (b) Axis-B (c) Axis-D
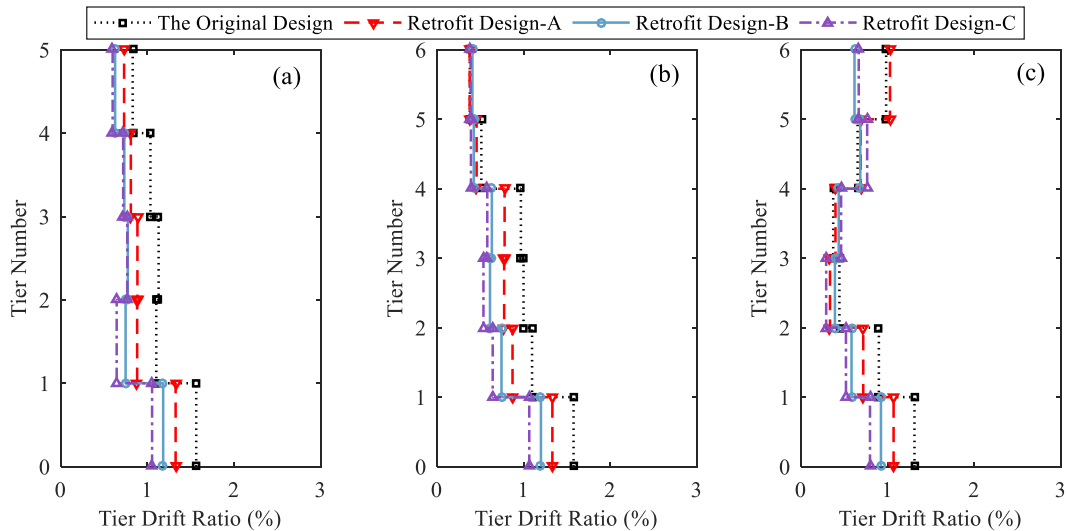
Fig. 15. Distributions of mean story drift ratios under 100%-MCE in Y-direction for columns in (a) Axis-A (b) Axis-B (c) Axis-D

The average of peak tier drift and residual tier drift over all considered intensities (i.e. 60% to 140% MCE) are shown in Fig. 16a and 16b, respectively. It is clear from Fig. 16a that the Original Design has the largest drift response among the four structures at each earthquake intensity. For the other three retrofit buildings, Retrofit Design-B experienced the smallest drift response under 60% MCE intensity and followed by Retrofit Design-C and Retrofit Design-A. The peak tier

400   drift is mainly determined by the results obtained from the 1st and 5th tiers of Axis-D in X-direction. Since there are no
401   added damping devices distributed in 1st to 5th tiers of Axis-D (Table 3), the peak tier drift of Retrofit Design-C is slightly
402   larger than the Retrofit Design-B. With the increase of ground motion intensity level, the results of the three retrofit
403   buildings are getting close and Retrofit Design-B turns to be the one experienced the largest peak drift demand under the
404   highest intensity level (i.e. 140% MCE). The result of residual drift distributions in Fig. 16b shows a different trend. Under
405   60% and 80% MCE excitations, the residual drift values of all designs are close. When the excitation intensity increases to
406   100% MCE, the mean residual drift value of the Original Design goes up to 0.24% while the values of the rest structures
407   are still below 0.2%. A significant increase in residual drift for the Original Design is observed when the excitation intensity
408   is beyond 100% MCE and it achieves at 0.9% at the end (i.e. 140% MCE). It is worth noting that Retrofit Design-B has a
409   sudden increase in residual drift response when the excitation intensity is greater than 100% MCE, which leads to a minimal
410   difference from the results of the Original Design. On the contrary, the retrofit structures that employed isolation for coal
411   bunkers (i.e. Retrofit Design-A and Retrofit Design-C) have smaller residual drift demands at the two highest excitation
412   levels.
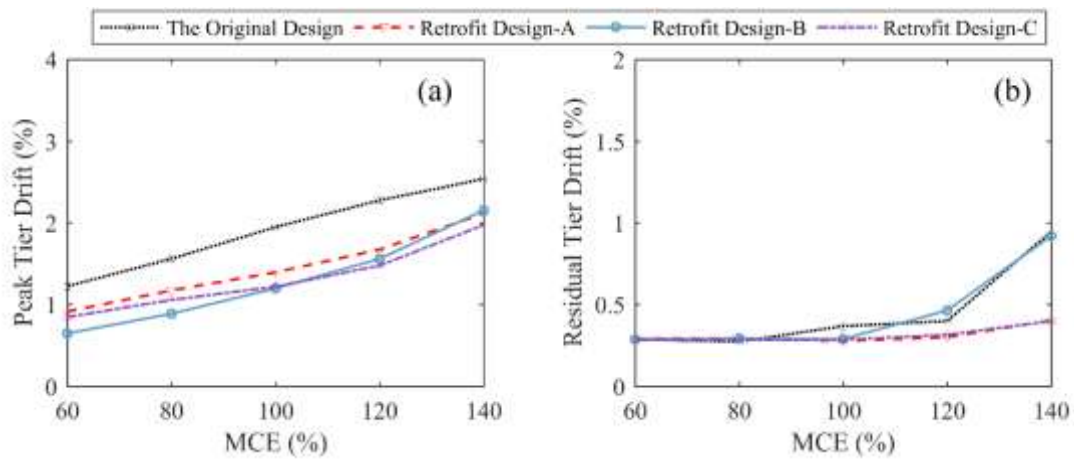
413
414   **Fig. 16.** Distribution profile of drift demands over 60% - 140% MCE intensities: (a) peak tier drift
415   (b) residual tier drift
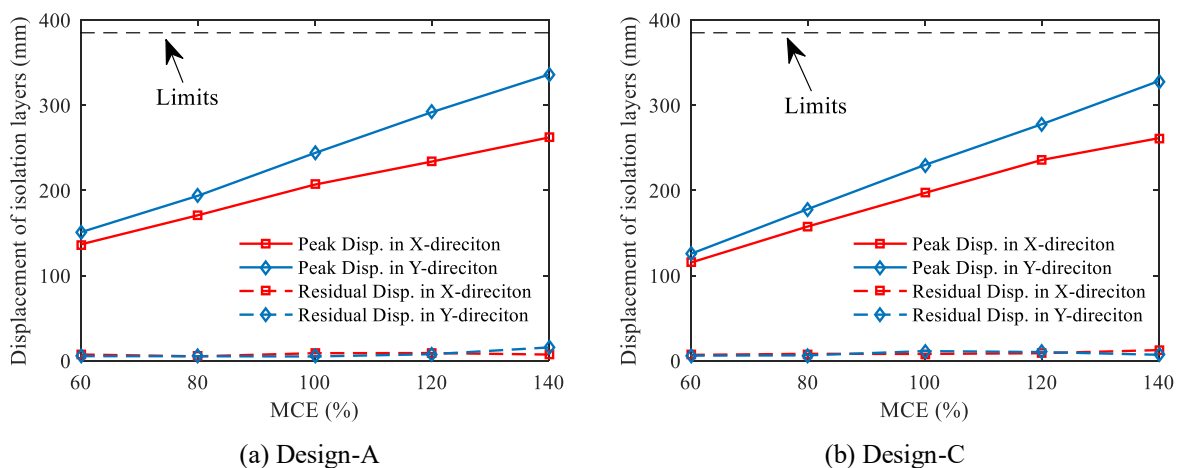
416
417   (a) Design-A   (b) Design-C
418   **Fig. 17.** Lateral displacement of isolation layers for coal bunkers
419   For the isolation layers of coal bunkers, the collisions between two adjacent coal bunkers and between coal bunkers
420   and structural/nonstructural components are not allowed. The peak and residual lateral displacements of the isolation layers
421   along X and Y direction over the considered intensities are plotted in Fig. 17. Recall that the maximum displacement

422 limitations for the isolation layers are 385 mm along both X direction and Y direction (Fig. 4). As seen in Fig. 17, the

423 maximum displacement in Y direction under the 140%MCE intensity is 335.9 and 328.3 mm for Retrofit Design-A and

424 Retrofit Design-C, respectively. Also, the permanent displacements of the isolation layer are 17 mm and 13 mm under

425 140% MCE earthquake level for Retrofit Design-A and Retrofit Design-C, respectively, which are acceptable for immediate

426 operation after earthquakes.

5.3 Probabilistic seismic demand model development

427

428 To derive the seismic risk, the probabilistic seismic demand model (PSDM) is first built to link the engineering demand

429 parameter (EDP) to the ground motion intensity measure (IM). A general mathematical formula of the seismic demand

430 model can be expressed by Equation (1) [49]. One of the most commonly used IMs is the spectral acceleration at the first-

431 mode period, $S_a(T_1)$. However, as evidenced by the obtained modal analysis results, the seismic behaviors of the TPP

432 building are not dominantly controlled by the first mode because of its highly structural complexity. Some researchers

433 proposed some alternatives of IM such as PGA, PGV, Aerial Intensity (AI) (e.g. [50]). In these prior studies, PGA is widely

434 suggested as the primary IM to measure the vulnerability of complex industrial buildings [51,52]. Therefore, in the current

435 study, PGA is used as the IM for the PSDM development. The peak tier story drift θ_{max} is considered as the EDP as it relates

436 well to damage states as suggested by modern performance assessment guidelines or tools (e.g. ASCE/SEI 41-13 [44],

437 Hazus-MH [53]). Based on the RHA results, a nonlinear regression analysis of the power-law form is performed to obtain

438 the required parameters of a, b (Equation (1)) as well as the dispersion of the demand $\beta_{EDP|IM}$ (Equation 2). An example of

439 the regression model based on the analysis results of the Original Design can be seen in Fig. 18. A comparison of the

440 demand models among the three retrofit designs and the Original Design is made in Fig. 19 and the associated demand

441 parameters are listed in Table 6. It is observed that when PGA is less than 0.75 g, the θ_{max} of Retrofit Design-B has the

442 smallest value and afterwards, it exceeds the values of Design-C. Additionally, the Design-B has a larger dispersion (i.e.

443 $\beta_{EDP|IM}$) than the other three models.

$$EDP = a \cdot IM^b \tag{1}$$

$$\beta_{EDP|IM} = \sqrt{\frac{\sum_{i=1}^{N}\left[\ln(EDP) - \ln(aIM^b)\right]^2}{N-2}} \tag{2}$$

444 where N is the number to total simulation cases.
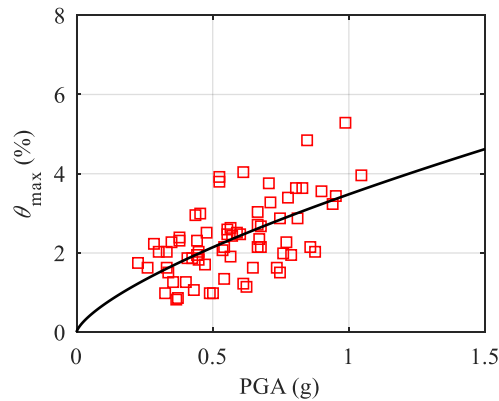
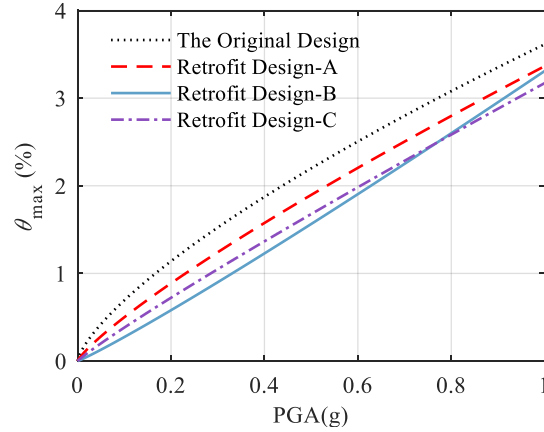Fig. 18. Probabilistic seismic demand model of the Original Design

Fig. 19. Comparison of the PSDMs for the four designed structures

### 5.4 Characterization of Damage States and Fragility Development

The probability of exceeding a damage state on the condition of *IM* can be expressed by fragility curves. The damage states for the TPP building are defined and each one represents a specific level of functionality. For SCBF systems, some popular performance-based guidelines such as the ASCE/SEI 41-13 [44] and FEMA 356 [54] have specified a series of discrete damage states, usually termed Immediate Occupancy (IO), Life Safety (LS) and Collapse Prevention (CP). The associate limit values for these damage states in terms of peak story drift are 0.5%, 1.5%, and 2%, respectively. Considering nonstructural components housed in the TPP building are different from residential buildings, three damages states that incorporate both structural components and industrial equipment are proposed as seen in Table 7.

A lognormal cumulative distribution function is used to model the seismic fragility which can be modeled as [55]:

$$P\big[D > C \mid IM = x\big] = 1 - \Phi\left[\frac{\ln(\hat{C} / \hat{D})}{\sqrt{\beta_{D|IM}^2 + \beta_C^2 + \beta_M^2}}\right] \tag{3}$$

where $\Phi[\cdot]$ is the standard normal probability integral; $\hat{C}$ is the median structural capacity associated with a certain limit state; $\hat{D}$ is the median seismic demands predicted by the PSDM; β_M and β_C represent the epistemic uncertainty in modeling and aleatoric uncertainty in seismic capacity (*C*), respectively.

The fragilities of all designed buildings for the considered three damage states (Table 7) are computed and compared in Fig. 20. The capacity and epistemic uncertainties, β_C and β_M are both assumed as 0.2 as suggested by Ellingwood *et al.* [55]. As seen in Fig. 20a, the differences among the results of the four designs are minimal. The median capacity of the Retrofit Design-B is 0.20g while the Original Design has a median capacity of 0.06g. The benefit of retrofit strategies becomes evident when it comes to the fragilities of DS2 and DS3. For example, the Original Design has the largest probability of exceedance for DS2 and DS3. The corresponding median capacities of the Original Design are 0.30g and 0.45g for DS2 and DS3, respectively. Compared to these results, the median capacities of Design-A and Design-B are 33% and 87% larger than that of DS2; 13% and 47% larger than that of DS3, respectively. The fragility result of Design-C is comparable to Design-B especially for DS3.
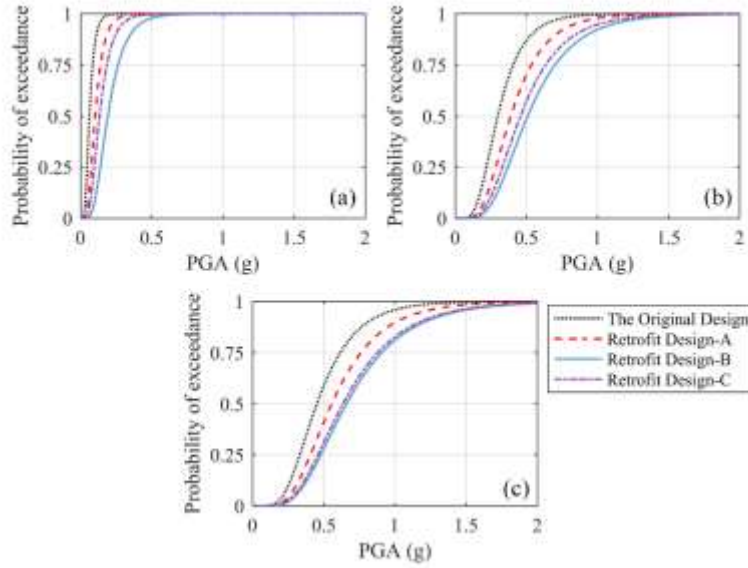
Fig. 20. Fragility curves of four designed structures for (a) DS1 (b) DS2 (c) DS3

5.5 Seismic risk and restoration analysis

The mean annual probability of exceedance for a certain damage state can be used to describe the seismic risk which is computed by:

$$\lambda_{DSi} = \int_0^\infty P(D > C_{DSi} \mid PGA = x) \cdot dH(x) \tag{4}$$

where $P(D > C_{DSi} \mid PGA = x)$ represents the probability of exceedance for a designated damage state when the *PGA* value is equal to *x*; $H(x)$ is the seismic hazard function described by the mean annual frequency for an earthquake incident with the *PGA* greater than *x*.

The site-specific seismic hazards (i.e. $H(x)$) where the actual TPP building is located are obtained with the help of MCPRC (2015) and are plotted in Fig. 21. The annual probability of exceedance in terms of θ_{max} for each design scheme are computed with Equation 4 and compared in Fig. 22. Consistent with the observations from PSDMs, the Retrofit Design-B has the smallest drift hazard, but it exceeds the results of Retrofit Design-A and Retrofit Design-C when θ_{max} = 2.4%. The drift hazards of the Original Design and Retrofit Design-A are close when θ_{max} is less than 0.6%. Assuming that the occurrence of earthquakes follows a Poisson process [57], the probability of exceeding the designated damage states over *t* years can be computed by using Equation (5). The results for a period of 50 years are presented in Table 8. Compared to the probability of exceeding DS3 for the Original Design, the seismic risk is reduced at most by 27%, 45%, and 41% for Retrofit Design-A, Retrofit Design-B, and Retrofit Design-C, respectively. The use of supplemental damping systems shows a greater benefit than the isolation of coal bunkers.

$$P(DSi \text{ in } t \text{ years}) = 1 - \exp(-\lambda_{DSi}t) \tag{5}$$
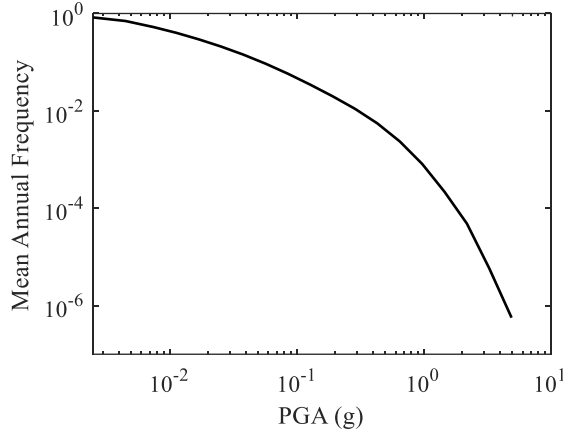
Fig. 21. Seismic hazard curve for the thermal power plant
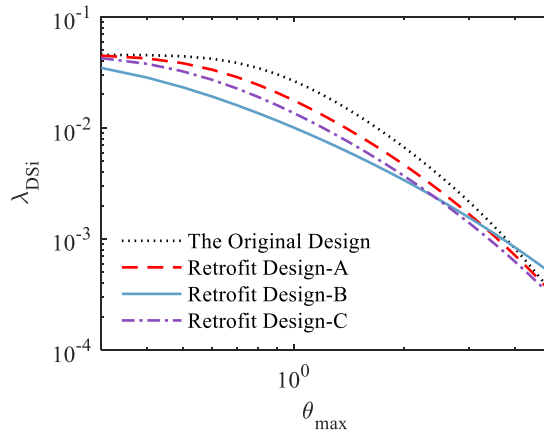
Fig. 22. Drift hazard levels for the four designs

The development of the performance-based theory allows the stakeholders to participate in decision making together with professional engineers. Downtime is one of the frequently used measures to describe the consequences of earthquakes. For electric power generation system, Hazus-MH [53] provided empirical models to estimate the downtime or recovery time from seismic damage. The expected downtime conditioned on a specific *IM* can be evaluated by using Equation (6). With the obtained structural fragilities (Fig. 20), the downtime over the variation of *PGA* values for four designs are compared in Fig. 23. Take an earthquake incident at MCE intensity level (i.e. *PGA* = 0.6g) as an example, the electric power restoration would cost 56 days, 49 days, 36 days, and 39 days for the Original Design, Retrofit Design-A, Retrofit Design-B, and Retrofit Design-C, respectively. It is noted that different from the seismic risk results, Retrofit Design-B and Retrofit Design-C have nearly the same downtime. Similarly, considering the site-specific seismic hazard, in a period of 50 years the downtime for the four structures are 26, 20, 15 and 17 days. Compared to the Original Design, the reduction of downtime induced by different retrofit strategies are 23.1%, 42.3%, and 34.6% for Retrofit Design-A, Retrofit Design-B, and Retrofit Design-C.

$$E(days \mid IM) = \sum_{i=1}^{i=3} E(days \mid DS_i) P(DS_i \mid IM) \tag{6}$$
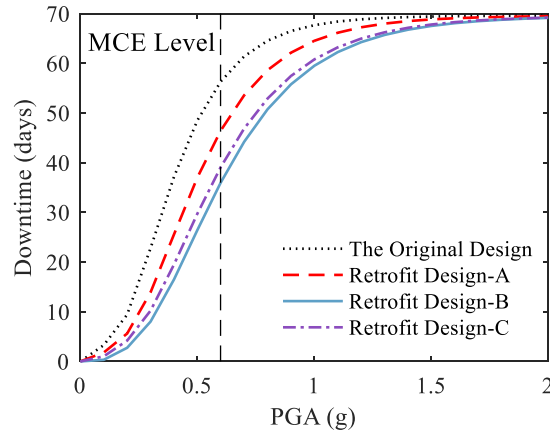
Fig. 23. Downtime estimation for different design schemes

6 Discussions and Research Significance

Based on the comparisons in seismic demands, the use of supplemental damping systems showed a better performance than others in terms of peak tier drift. However, it is noted that the Retrofit Design-B has a comparable result with the Original Design for residual tier drift demands when the earthquake intensity is greater than 100%MCE level. This is partly due to the hysteric properties of the metallic damping devices. This shortcoming regarding residual deformation left after earthquake was also a concern in plenty of studies (e.g. [58–60]) and consequently, self-centering braces and innovative systems were proposed to eliminate the permanent deformation (e.g. [61,62]). In contrast, the Retrofit Design-A and Retrofit Design-C which have used isolation for coal bunkers experienced larger peak drift responses but left smaller residual drifts. Additionally, the residual displacement of the isolation layers is minimal enough for immediate operation even after an earthquake at 140% MCE level. When it comes to the structural damage quantified by peak drift demands, the associated repair costs for the Retrofit Design-A and Retrofit Design-C are likely larger than the Retrofit Design-B. But extra costs related to the replacement of damping devices are inevitable for the Retrofit Design-B. A detailed comparison in the aspect of detailed cost-benefit analysis is of interest in actual engineering projects.

Since economic loss is an important measure to describe the consequences caused by earthquakes, a non-structural building model is needed together with the corresponding structural system. The nonstructural system housed in the TPP building includes a variety of components such as generators, turbines, racks, vessels, panels, pipelines. In some modern performance-based guidelines, most stipulations associated with nonstructural elements are only applicable for residential and commercial buildings. The knowledge gap which lies in the seismic damage of industrial equipment warrants more efforts in the future. In this study, the seismic risk was assessed mainly in the aspect of the structural system. The damage states of some common industrial components are considered in this study (Table 7). However, it is a rough consideration. More detailed elaboration is required in further studies. If so, the retrofit system design would be performed based on the responses in both structural components and critical operational facilities. In addition, the interaction between coal material and the bunkers is not only normally ignored in seismic design as prescribed in guidelines [8,9] but also in prior studies in which similar silo-shape structures were focused [23,63]. Such issue is suggested to be studied in the future.

The industrial equipment housed in the TPP building are arranged in a typical way to serve to the physical power generation process. Therefore, the structural system is designed in a standard form like the building focused in this study. The proposed retrofit schemes and the seismic risk assessment framework are expected to be explicitly refereed by practical professionals when doing similar engineering projects. Also, as presented in this study, the benefits in terms of seismic risk

535 and downtime reduction from using damping and isolation techniques help stakeholders and social governors make

536 thorough decisions regarding the retrofit strategy selection.

7 Conclusions

538 Considering the essential role of the thermal power plant in an urban city, the performance of an actual TPP building

539 retrofitted by different resilient strategies was assessed in this paper. The structural system of the TPP building is usually

540 characterized by irregularities because of the operational constraints. To enhance its seismic performance, the isolation

541 technique was employed to mitigate the detrimental effect of heavy coal bunkers. Also, the metallic low-point-yielding

542 damping systems (i.e. YSPD and BRB) were considered as an alternative strategy. A total of three retrofit design schemes

543 were proposed: The Retrofit Design-A used the isolation of coal bunkers only; Retrofit Design-B used the added damping

544 systems only; and Retrofit Design-C used both isolation of coal bunkers and added damping systems. The performance of

545 the Original Design which adopted SCBF as LRFS was taken as the baseline. The seismic demands of each designed

546 structure were obtained from nonlinear RHAs. Subsequently, the benefit of each retrofit scheme was quantified in terms of

547 seismic risk and downtime.

548 The seismic demands of structural frames along the two principal directions were compared. The peak drift profiles

549 showed that the retrofit design schemes have smaller drift demands than the Original Design, especially for the critical

550 tiers. The use of damping systems showed better performance than the isolation of coal bunkers in terms of peak tier drifts.

551 However, under an earthquake intensity that beyond MCE, the performance of Design-B turned to be worse than the other

552 two retrofit designs both in terms of peak tier drift and residual tier drift.

553 Based on the nonlinear RHA results, PSDMs and seismic fragilities corresponding to the proposed three damage states

554 were developed. For Retrofit Design-B, the predicted demands using PSDM were smaller than other design schemes when

555 *PGA* is below 0.75g. But Retrofit Design-B has the largest dispersion in drift demands which signifies the structural system

556 with added damping devices is more susceptible to the record-to-record variety than the use of coal bunker isolations. The

557 fragility results showed that the benefit of the considered retrofit strategies raises with the severity of structural damage

558 states. Compared with the Original Design, the introduction of isolation for coal bunkers and added damping system

559 increased the median seismic capacities at most by 29% and 62%. Convoluting the seismic fragilities with the site-specific

560 hazard, the seismic risk results were obtained. The isolations for coal bunkers and added damping systems helped to

561 mitigate the seismic risk by 19% and 38%, respectively. The seismic risk of the combined retrofit design scheme (i.e.

562 Retrofit Design-C) is comparable to that of Retrofit Design-B. The downtime for all the considered design schemes were

563 obtained and compared to reflect the benefit of different retrofit strategies in post-earthquake recovery. Retrofit Design-B

564 and Retrofit Design-C have close results in downtime which is approximately 20 days less than that of the Original Design

565 if considering a single earthquake incident at the MCE intensity. Over a period of 50 years, the reductions of downtime are

566 23.1%, 42.3%, and 34.6% due to the use of isolation for coal bunkers, added damping system, and combined use of isolation

567 and damping system, respectively.

568 Overall, for the TPP building considered in this study, the coal bunker isolation is less effective in the improvement

569 of seismic performance and seismic risk than added damping systems. Under an earthquake event with an intensity greater

570 than MCE level, the added damping systems failed to reduce the residual drift demands which leads to a high likelihood

571 of demolishment in the aftermath of the earthquake. The effectiveness of the combined use of isolation and damping system

572 techniques is between the former two schemes. The selection of the retrofit strategies is suggested to be made based on the

573 opinions of structural engineers, stakeholders as well as professionals across other disciplines. This study could be

574 profitably used as an example for further seismic risk evaluation for an industrial building equipped with resilient systems

575 in practice.

576

582

583 **Reference**

584 [1] Eshghi S, Razzaghi MS. Performance of Industrial Facilities in the 2003 Bam , Iran , Earthquake. Earthq Spectra

585   2005;21:395–410. doi:10.1193/1.2098810.

586 [2] Cruz EF, Valdivia D. Performance of industrial facilities in the Chilean earthquake of 27 February 2010. Struct

587   Des Tall Spec Build 2011;20:83–101. doi:10.1002/tal.679.

588 [3] Fujita S. Seismic damage of mechanical structures by the 2011 Great East Japan Earthquake. 15th World Conf.

589   Earthq. Eng., Lisbon,Portugal: 2012.

590 [4] Bournas DA, Negro P, Taucer FF. Performance of industrial buildings during the Emilia earthquakes in Northern

591   Italy and recommendations for their strengthening. Bull Earthq Eng 2014;12:2383–404.

592 [5] Rossi E, Ventrella M, Faggella M, Gigliotti R, Braga F. Performance based earthquake assessment of an

593   industrial silos structure and retrofit with sliding isolators. ECCOMAS Congr 2016 - Proc 7th Eur Congr Comput

594   Methods Appl Sci Eng 2016;3:5–10. doi:10.7712/100016.2229.11993.

595 [6] Erdem HH, Akkaya AV, Cetin B, Dagdas A, Sevilgen SH, Sahin B, et al. Comparative energetic and exergetic

596   performance analyses for coal-fired thermal power plants in Turkey. Int J Therm Sci 2009;48:2179–86.

597   doi:10.1016/j.ijthermalsci.2009.03.007.

598 [7] World Coal Association. Coal and Electricity 2015.

599 [8] ASCE. ASCE 7-10 Minimum design loads for buildings and other structures. Reston, VA: American Society of

600   Civil Engineers; 2010.

601 [9] CEN. Eurocode 8: design of structures for earthquake resistance Part 1: general rules, seismic actions and rules

602   for buildings (EN 1998-1). Brussels: European Committee of Standardization; 2013.

603 [10] NCh. Earthquake Resistant Design of Industrial Structures and Facilities NCh 2369. Chilean Ministry of

604   Housing; 2003.

605 [11] Ellingwood BR. Earthquake risk assessment of building structures. Reliab Eng Syst Saf 2001;74:251–62.

606   doi:10.1016/S0951-8320(01)00105-3.

607 [12] Rojas HA, Foley C, Pezeshk S. Risk-based seismic design for optimal structural and nonstructural system

608   performance. Earthq Spectra 2011;27:857–80. doi:10.1193/1.3609877.

609 [13] Hwang SH, Lignos DG. Earthquake-induced loss assessment of steel frame buildings with special moment

610   frames designed in highly seismic regions. Earthq Eng Struct Dyn 2017;46:2141–62. doi:10.1002/eqe.2898.

611 [14] Ramirez CM, Miranda E. Significance of residual Drifts in building earthquake loss estimation. Earthq Eng

612   Struct Dyn 2012;41:1477–93.

613 [15] Lu D, Yu X, Jia M, Wang G. Seismic risk assessment for a reinforced concrete frame designed according to

614   Chinese codes. Struct Infrastruct Eng 2013:1–16. doi:10.1080/15732479.2013.791326.

615 [16] Tubaldi E, Barbato M, Dall'Asta A. Performance-based seismic risk assessment for buildings equipped with

616   linear and nonlinear viscous dampers. Eng Struct 2014;78:90–9. doi:10.1016/j.engstruct.2014.04.052.

617 [17] Hossain MR, Ashraf M, Padgett JE. Risk-based seismic performance assessment of Yielding Shear Panel Device.

618   Eng Struct 2013;56:1570–9. doi:10.1016/j.engstruct.2013.07.032.

619 [18] Tafakori E, Banazadeh M, Jalali SA, Tehranizadeh M. Risk-Based Optimal Retrofit of a Tall Steel Building By

620   Using Friction Dampers. Struct Des Tall Specail Build 2013;22:700–17.

621 [19] Liel AB, Deierlein GG. Cost-Benefit Evaluation of Seismic Risk Mitigation Alternatives for Older Concrete

622   Frame Buildings. Earthq Spectra 2013;29:1391–411. doi:10.1193/030911EQS040M.

623 [20] Han R, Li Y, van de Lindt J. Seismic risk of base isolated non-ductile reinforced concrete buildings considering

624   uncertainties and mainshock-aftershock sequences. Struct Saf 2014;50:39–56.

625   doi:10.1016/j.strusafe.2014.03.010.

626 [21] Colombo JI, Almazán JL. Seismic reliability of continuously supported steel wine storage tanks retrofitted with

627   energy dissipation devices. Eng Struct 2015;98:201–11. doi:10.1016/j.engstruct.2015.04.037.

628 [22] Kanyilmaz A, Castiglioni CA. Reducing the seismic vulnerability of existing elevated silos by means of base

629   isolation devices. Eng Struct 2017;143:477–97. doi:10.1016/j.engstruct.2017.04.032.

630 [23] Pinkawa M, Hoffmeister B, Feldmann M. Performance Assessment of Seismic Retrofitting Measures on Silo

631   Structures Using Innovative Seismic Protection Systems. Proc. VII Eur. Congr. Comput. Methods Appl. Sci.

632   Eng. (ECCOMAS Congr. 2016), 2016, p. 5851–67. doi:10.7712/100016.2225.8876.

633 [24] Paolacci F, Giannini R, Angelis M De. Seismic response mitigation of chemical plant components by passive

634   control techniques. J Loss Prev Process Ind 2013;26:924–35. doi:10.1016/j.jlp.2013.03.003.

635 [25] Wang J, Dai K, Yin Y, Tesfamariam S. Seismic performance-based design and risk analysis of thermal power

636   plant building with consideration of vertical and mass irregularities. Eng Struct 2018;164:141–54.

637   doi:10.1016/j.engstruct.2018.03.001.

638 [26] Chanand RW, Zhao Z. Mitigation of Seismic Risks To Soft-Storey Structures Using Toggle-Brace-Damper

639   Systems. Appl Mech Mater 2012;238:833–7. doi:10.4028/www.scientific.net/AMM.238.833.

640 [27] Wanitkorkul A, Filiatrault A. Influence of passive supplemental damping systems on structural and nonstructural

641   seismic fragilities of a steel building. Eng Struct 2008;30:675–82. doi:10.1016/j.engstruct.2007.05.013.

642 [28] Karamanci E, Lignos DG. Computational Approach for Collapse Assessment of Concentrically Braced Frames in

643   Seismic Regions. J Struct Eng 2014;140:A4014019. doi:10.1061/(ASCE)ST.1943-541X.0001011.

644 [29] Sabelli R, Mahin S, Chang C. Seismic demands on steel braced frame buildings with buckling-restrained braces.

645   Eng Struct 2003;25:655–66. doi:10.1016/S0141-0296(02)00175-X.

646 [30] Chan RWK, Albermani F, Kitipornchai S. Experimental study of perforated yielding shear panel device for

647   passive energy dissipation. J Constr Steel Res 2013;91:14–25. doi:10.1016/j.jcsr.2013.08.013.

648 [31] Uckan E, Akbas B, Shen J, Wen R, Turandar K, Erdik M. Seismic performance of elevated steel silos during Van

649   earthquake, October 23, 2011. Nat Hazards 2015;75:265–87. doi:10.1007/s11069-014-1319-9.

650 [32] Fell B V., Kanvinde AM, Deierlein GG, Myers AT. Experimental Investigation of Inelastic Cyclic Buckling and

651   Fracture of Steel Braces. J Struct Eng 2009;135:19–32. doi:10.1061/(ASCE)0733-9445(2009)135:1(19).

652 [33] Dai K, Li B, Wang J, Li A, Li H, Li J, et al. Optimal probability-based partial mass isolation of elevated coal

653   scuttle in thermal power plant building. Struct Des Tall Spec Build 2018;27:e1477. doi:10.1002/tal.1477.

654   [34]   AISC. AISC 360-10 Specifications for structural steel buildings. ANSI/AISC. Chicago: American Institute of
655   Steel Construction; 2010.

656   [35]   AISC. AISC 341-10 Seismic provisions for structural steel buildings. ANSI/AISC. Chicago: American Institute
657   of Steel Construction; 2010.

658   [36]   Lehman DE, Roeder CW, Herman D, Johnson S, Kotulka B. Improved Seismic Performance of Gusset Plate
659   Connections. J Struct Eng 2008;134:890–901. doi:10.1061/(ASCE)0733-9445(2008)134:6(890).

660   [37]   Hao L, Zhang R, Jin K. Direct design method based on seismic capacity redundancy for structures with metal
661   yielding dampers. Earthq Eng Struct Dyn 2018;47:515–34. doi:10.1002/eqe.2977.

662   [38]   CSI. SAP2000 Version 18. Optimized Modeling and Design of Structures Using SAP2000. 2015.

663   [39]   Asghari A, Gandomi AH. Ductility reduction factor and collapse mechanism evaluation of a new steel knee
664   braced frame. Struct Infrastruct Eng 2016;12:239–55. doi:10.1080/15732479.2015.1009123.

665   [40]   Balendra T, Sam M-T, Liaw C-Y, Lee S-L. Preliminary studies into the behavior of knee braced frames subject
666   to seismic loading. Eng Struct 1991;13:67–74.

667   [41]   Junda E, Leelataviwat S, Doung P. Cyclic testing and performance evaluation of buckling-restrained knee-braced
668   frames. J Constr Steel Res 2018;148:154–64. doi:10.1016/j.jcsr.2018.05.012.

669   [42]   Leelataviwat S, Suksan B, Srechai J, Warnitchai P. Seismic Design and Behavior of Ductile Knee-Braced
670   Moment Frames. J Struct Eng 2011;137:579–88. doi:10.1061/(ASCE)ST.1943-541X.0000301.

671   [43]   CSI. Nonlinear analysis and performance assessment for 3D structures 2013.

672   [44]   ASCE. Seismic Evaluation and Retrofit of Existing Buildings ASCE/SEI 41-13. Reston, VA: American Society
673   of Civil Engineers; 2014.

674   [45]   Powell J. Evaluation of special concentrically braced frames for improved seismic performance and
675   constructability (Master thesis). University of Washington, 2010.

676   [46]   Liu K, Dai K, Li A, Li H, Wang J, Li B. Shaking table test model design of a large complex power plant
677   structure. 264th China Eng. Sci. Technol. Forum 10th Natl. Conf. Earthq. Disaster Prev. Mitig. Eng., Chengdu,
678   China: 2018.

679   [47]   Speicher MS, Harris JL. Collapse Prevention seismic performance assessment of new buckling-restrained braced
680   frames using ASCE 41. Eng Struct 2018;164:274–89. doi:10.1016/j.engstruct.2018.01.067.

681   [48]   PEER. Pacific Earthquake Engineering Research Center PEER Ground Motion Database 2018.
682   http://ngawest2.berkeley.edu/.

683   [49]   Cornell CA, Jalayer F, Hamburger RO, Foutch DA. Probabilistic Basis for 2000 SAC Federal Emergency
684   Management Agency Steel Moment Frame Guidelines. J Struct Eng 2002;128:526–33.
685   doi:10.1061/(ASCE)0733-9445(2002)128:4(526).

686   [50]   Giovenale P, Ciampoli M, Jalayer F. Comparison of ground motion intensity measures using the incremental
687   dynamic analysis. In: Kiureghian D, editor. Appl. Stat. Probab. Civ. Eng., Madanat & Pestana (eds); 2003.

688   [51]   Panico A, Basco A, Lanzano G, Pirozzi F, Santucci de Magistris F, Fabbrocino G, et al. Evaluating the structural
689   priorities for the seismic vulnerability of civilian and industrial wastewater treatment plants. Saf Sci 2017;97:51–
690   7. doi:10.1016/j.ssci.2015.12.030.

691   [52]   Salzano E, Garcia Agreda A, Di Carluccio A, Fabbrocino G. Risk assessment and early warning systems for
692   industrial facilities in seismic zones. Reliab Eng Syst Saf 2009;94:1577–84. doi:10.1016/j.ress.2009.02.023.

693   [53]   Hazus. Hazus–MH 2.1: Technical Manual. 2012.

694　[54]　FEMA. Prestandard and commentray for the seismic rehabilitation of buildings. Washington, DC: Federal

695　　　　　Emergency Management Agency; 2000.

696　[55]　Ellingwood BR, Celik OC, Kinali K. Fragility assessment of building structural systems in Mid-America. Earthq

697　　　　　Eng Struct Dyn 2007;36:1935–52. doi:10.1002/eqe.693.

698　[56]　MCPRC. Seismic ground motion parameters zonation map of China. Beijing, China: Ministry of Construction of

699　　　　　Peoples Republic of China; 2015.

700　[57]　Cornell CA. Engineering seismic risk analysis. Bull Seismol Soc Am 1968;58:1583–606.

701　[58]　Erochko J, Christopoulos C, Tremblay R, Choi H. Residual Drift Response of SMRFs and BRB Frames in Steel

702　　　　　Buildings Designed according to ASCE 7-05. J Struct Eng 2011;137:589–99. doi:10.1061/(ASCE)ST.1943-

703　　　　　541X.0000296.

704　[59]　Deylami A, Mahdavipour MA. Probabilistic seismic demand assessment of residual drift for Buckling-Restrained

705　　　　　Braced Frames as a dual system. Struct Saf 2016;58:31–9. doi:10.1016/j.strusafe.2015.08.004.

706　[60]　Kiggins S, Uang CM. Reducing residual drift of buckling-restrained braced frames as a dual system. Eng Struct

707　　　　　2006;28:1525–32. doi:10.1016/j.engstruct.2005.10.023.

708　[61]　Guan X, Burton H, Moradi S. Seismic performance of a self-centering steel moment frame building: From

709　　　　　component-level modeling to economic loss assessment. J Constr Steel Res 2018;150:129–40.

710　　　　　doi:10.1016/j.jcsr.2018.07.026.

711　[62]　Tremblay R, Lacerte M, Christopoulos C. Seismic Response of Multistory Buildings with Self-Centering Energy

712　　　　　Dissipative Steel Braces. J Struct Eng 2008;134:108–20. doi:10.1061/(ASCE)0733-9445(2008)134:1(108).

713　[63]　Merino Vela RJ, Brunesi E, Nascimbene R. Derivation of floor acceleration spectra for an industrial liquid tank

714　　　　　supporting structure with braced frame systems. Eng Struct 2018;171:105–22.

715　　　　　doi:10.1016/j.engstruct.2018.05.053.

716

717

718   **Table 1.** Parameters of isolator device for coal bunker isolation

Outer bounded rubber diameter (mm)	Initial stiffness, K_0 (kN/mm)	Post-yield stiffness, K_F (kN/mm)	Yielding strength, F_Y (kN)	Vertical stiffness, K_V (kN/mm)	Allowable deformation
700	9.97	0.77	106	3509	385

719

720

Table 2. The arrangement of supplemental damping systems in Design-B

Frame	Tier Number	Damping Device	Quantity	Yielding Strength (kN)	Initial Stiffness (kN/mm)
Axis-A and B	1	YSPD	2	1,800	1,200
	2		2	1,500	1,000
	3		2	1,000	667
Axis-C and D	2	YSPD	2	2,000	1,333
	3	BRB	4	2,500	1,250
	4		4	3,000	1,500
	5	YSPD	2	1,800	1,200
	7	YSPD	2	1,200	800
Axis-1 to Axis-8	1	BRB	1	4,500	2,250
	2	BRB	1	4,500	2,250
	3	YSPD	2	1,200	800
	5	YSPD	1	1,200	800

721

722

Table 3. The arrangement of supplemental damping systems in Design-C

Frame	Tier Number	Damping Device	Quantity	Yielding Strength (kN)	Initial Stiffness (kN/mm)
Axis-A and B	2	YSPD	2	1,200	800
	3		2	800	533
Axis-C and D	6	YSPD	2	1,500	1,000
Axis-1 to Axis-8	1	BRB	1	4,500	2,250
	2	BRB	1	4,500	2,250

723

Table 4. Information of the first three modes of the TPP building

Mode	The Original Design	Retrofit design-A	Retrofit design-B	Retrofit design-C
1	2.00	2.04	1.95	1.97
2	1.50	1.62	1.30	1.33
3	0.84	1.12	1.08	1.11

Table 5. Summary of the selected ground motions

No.	Earthquake name	Year	Station name	Mw	Rrup (km)	Vs30 (m/s)	MSE
1	Borrego	1942	El Centro Array #9	6.5	56.9	213.4	9.40%
2	El Alamo	1956	El Centro Array #9	6.8	121.7	213.4	8.21%
3	Friuli Italy-02	1976	Codroipo	5.9	41.4	249.3	6.67%
4	Imperial Valley-06	1979	Calipatria Fire Station	6.5	24.6	205.8	8.65%
5	Imperial Valley-06	1979	Delta	6.5	22.0	242.1	2.72%
6	Imperial Valley-06	1979	El Centro Array #13	6.5	22.0	249.9	7.97%
7	Superstition Hills-02	1987	Imperial Valley Wildlife Liquefaction Array	6.5	23.9	179.0	7.73%
8	Loma Prieta	1989	Agnews State Hospital	6.9	24.6	239.7	8.57%
9	Loma Prieta	1989	Dumbarton Bridge West End FF	6.9	35.5	238.1	8.89%
10	Loma Prieta	1989	Hollister Differential Array	6.9	24.8	215.5	5.56%
11	Taiwan SMART1(45)	1986	SMART1 I01	7.3	56.2	275.8	8.12%
12	Chi-Chi Taiwan	1999	CHY015	7.6	38.1	228.7	9.89%
13	Manjil Iran	1990	Rudsar	7.4	64.5	242.1	9.42%
14	Hector Mine	1999	12440 Imperial Hwy North Grn	7.1	176.6	276.4	7.83%
15	Hector Mine	1999	Newhall - Fire Sta	7.1	198.1	269.1	7.04%

727

Table 6 Parameter values of the PSDMs for the four designed structures

Design Scheme	a	b	β
Original Design	3.48	0.70	0.36
Retrofit Design-A	3.23	0.82	0.37
Retrofit Design-B	3.18	1.12	0.42
Retrofit Design-C	2.99	0.89	0.39

729

Table 7 Damage states considered for the TPP building

Damage State	Structural Elements	Nonstructural Elements
DS1: slight damage	Minor yielding or buckling of braces. Peak tier drift θ_{max} exceeds 0.5%	Turbine tripping, light damage to electric generators
DS2: moderate damage	Many braces yield and buckle but do not totally fail. Many connections may fail. Peak tier drift θ_{max} exceeds 1.5%	Instrument panels and racks sliding, but no overturning; some realignment required to operate; considerable damage to pressure vessels or considerable damage to vertical pumps for deaerator and feedwater heater
DS3: extensive damage	Extensive yielding and buckling of braces. Many braces and their connections may fail. Peak tier drift θ_{max} exceeds 2%	Extensive damage to large horizontal vessels beyond repair; extensive damage to anchored supports of large equipment such as deaerator and feedwater heater; Sensitive equipment such as generators and condensors being unfunctional; Some pipelines rupture.

732

Table 8 Probability of exceeding damage states over 50 years for the four designs

Damage State	The Original Design	Retrofit Design-A	Retrofit Design-B	Retrofit Design-C
DS1	89.0%	85.2%	68.7%	80.1%
DS2	47.5%	34.9%	24.0%	28.3%
DS3	28.4%	20.7%	15.5%	16.8%

733

① Steam Turbine
② Surface Condenser
③ Electric Generator
④ Deaerator
⑤ Feedwater heater
⑥ Coal Conveyor
⑦ Coal Bunker
⑧ Coal pulverizer
⑨ Pipelines and auxiliary equipment

Turbine Hall — Deaerator Bay — Bunker Bay

TAL_1719_Figure1.tif

(a)

(b)

(c)

(d)

(e)

(f)

TAL_1719_Figure2.tif

TAL_1719_Figure3.tif

Chevron-bracing connection **X-bracing connection**
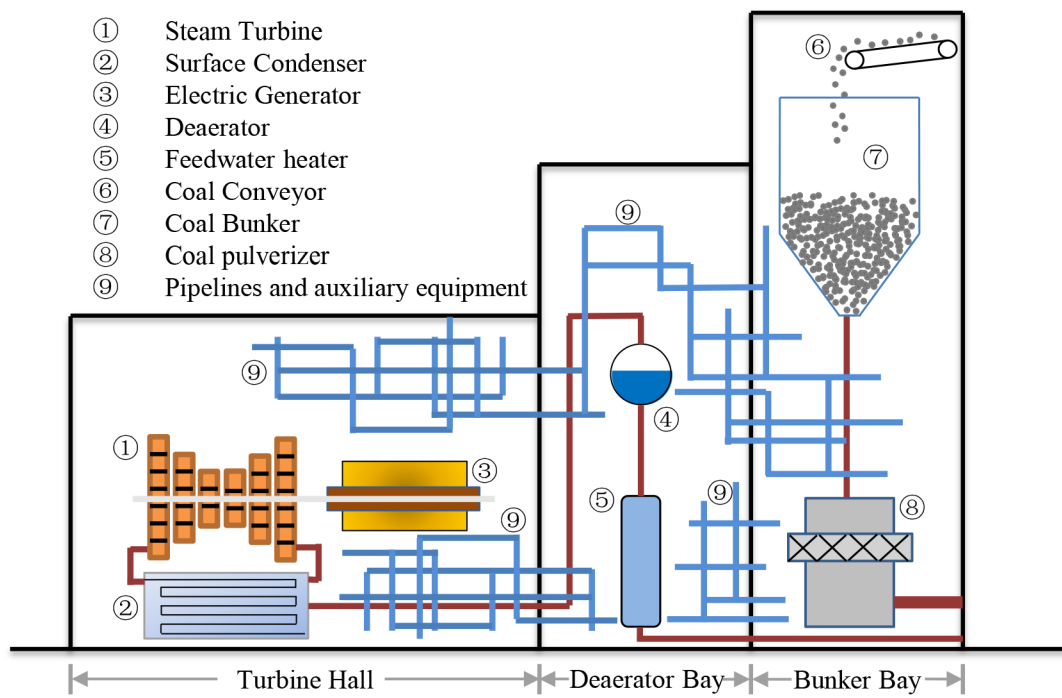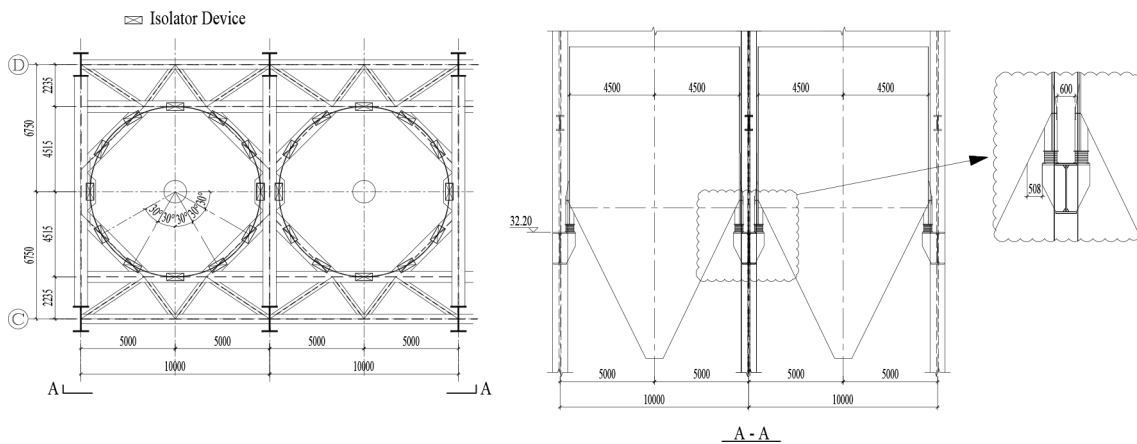
YSPD
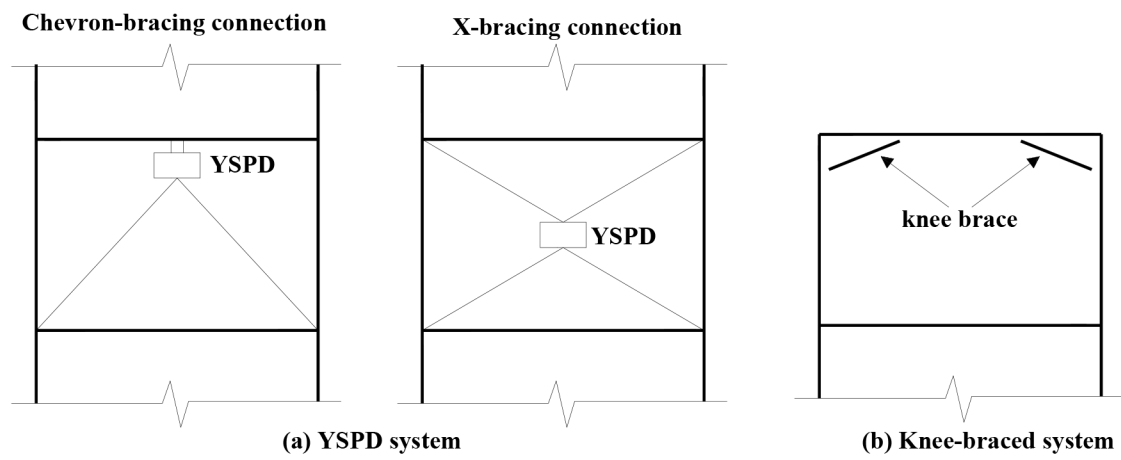
YSPD

knee brace

(a) YSPD system (b) Knee-braced system

TAL_1719_Figure4.tif

(a)

(b)

(c)
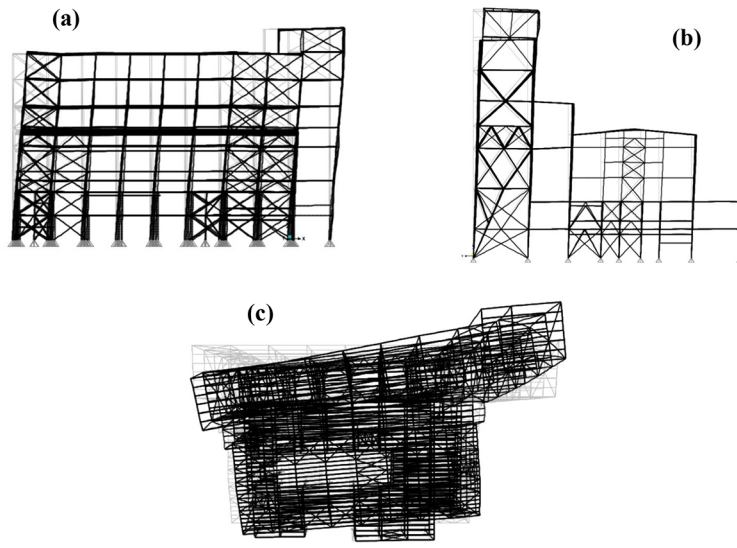
TAL_1719_Figure5.tif

TAL_1719_Figure7.tif

Coal bunker supporters
Center of mass of a coal bunker
Beam components
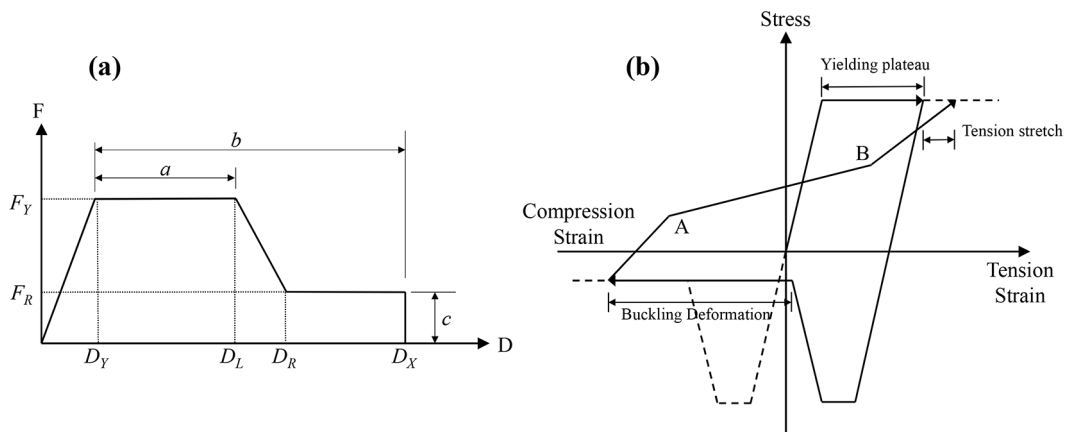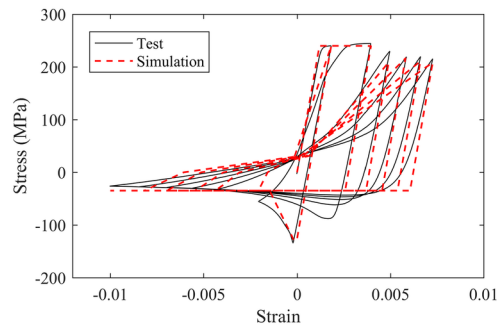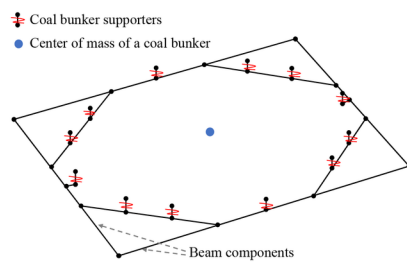
TAL_1719_Figure8.tif
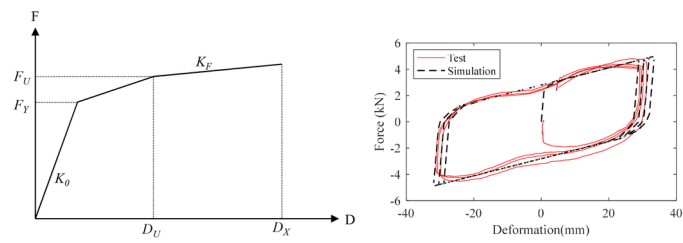
TAL_1719_Figure9.tif
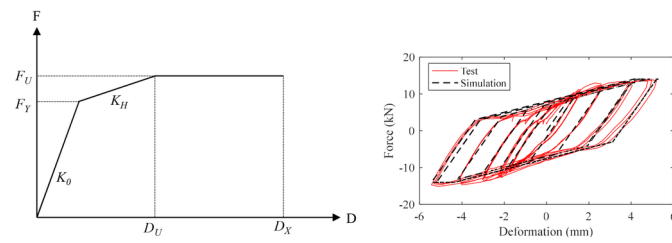
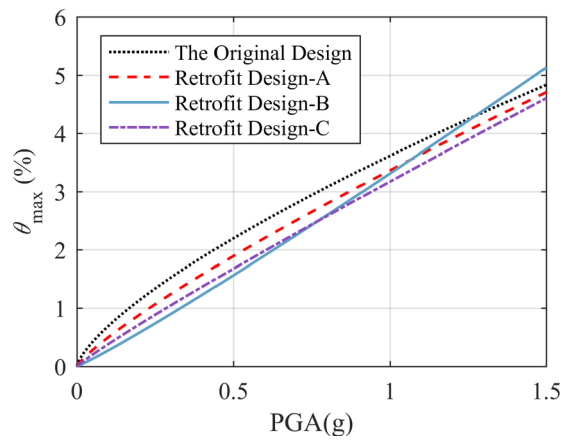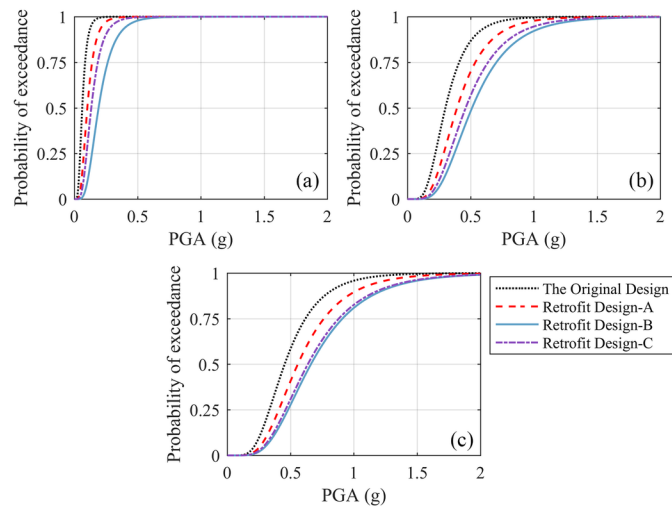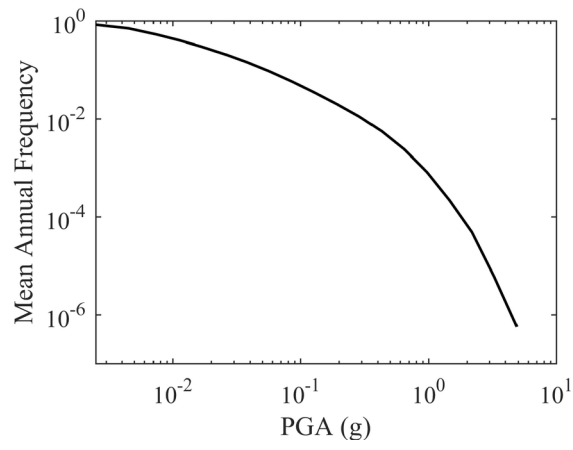TAL_1719_Figure10.tif
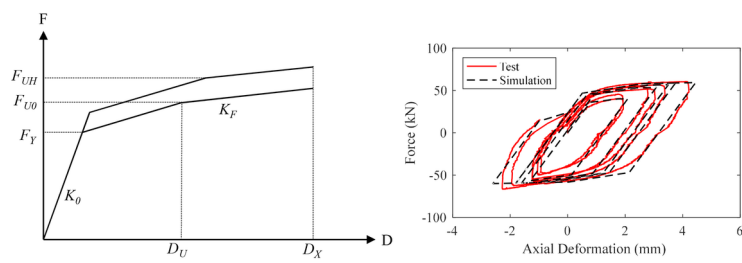
TAL_1719_Figure11.tif
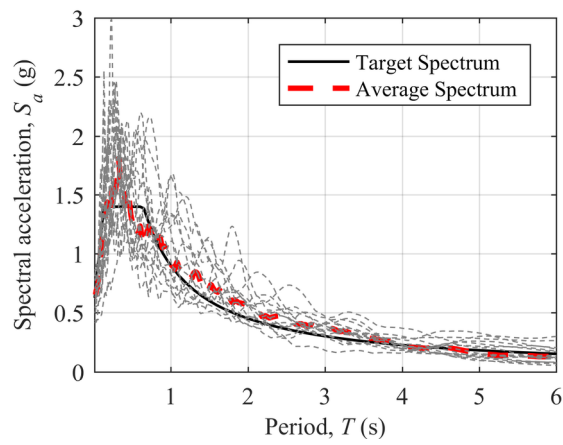
TAL_1719_Figure12.tif

TAL_1719_Figure13.tif

The Original Design .... Retrofit Design-A ---- Retrofit Design-B —○— Retrofit Design-C ·—·—·

(a) Tier Drift Ratio (%)

(b) Tier Drift Ratio (%)

(c) Tier Drift Ratio (%)
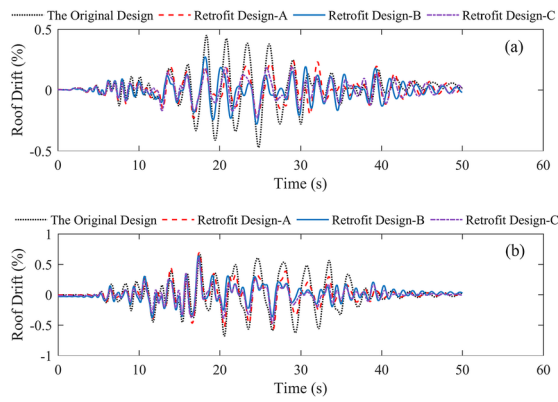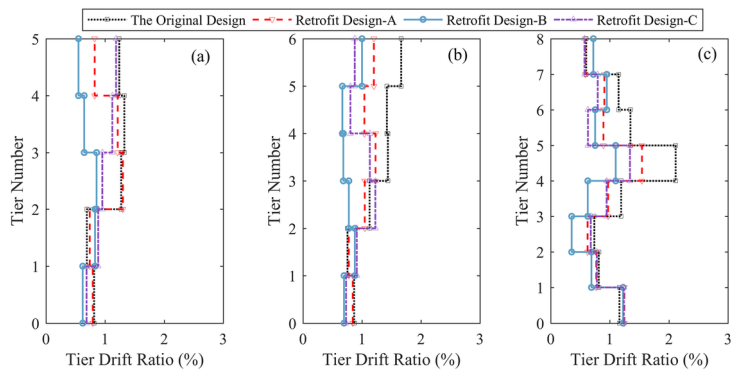
TAL_1719_Figure14.tif
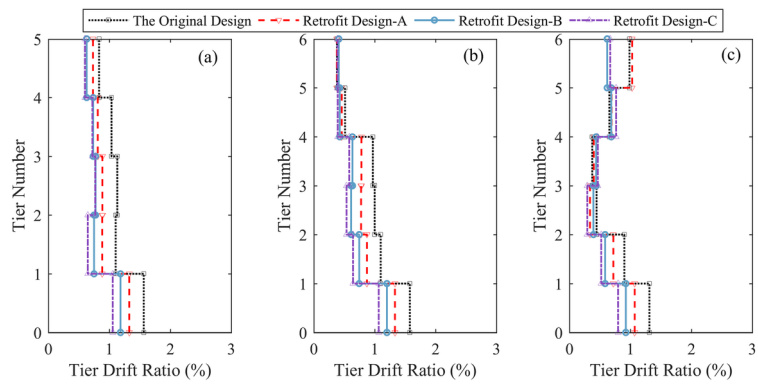
TAL_1719_Figure15.tif
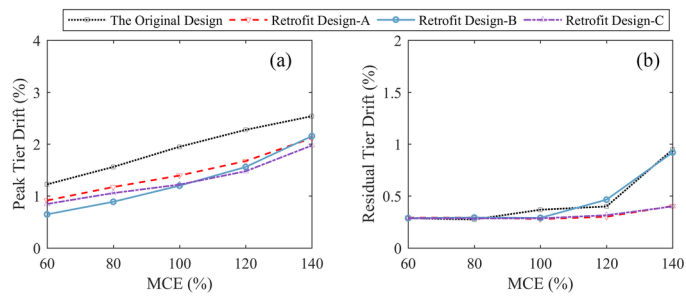
TAL_1719_Figure16.tif
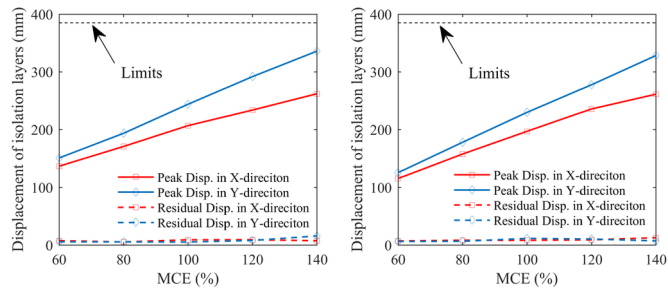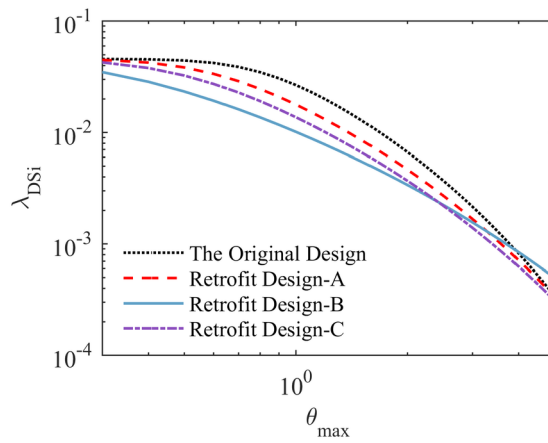
TAL_1719_Figure17.tif
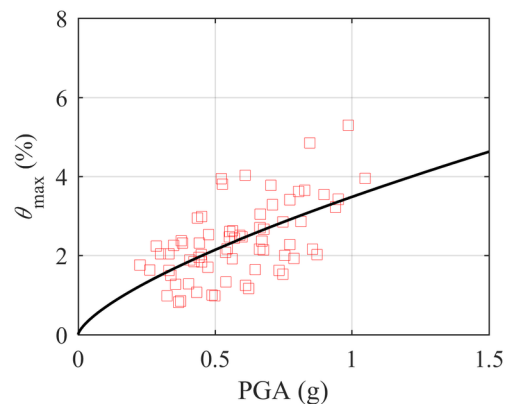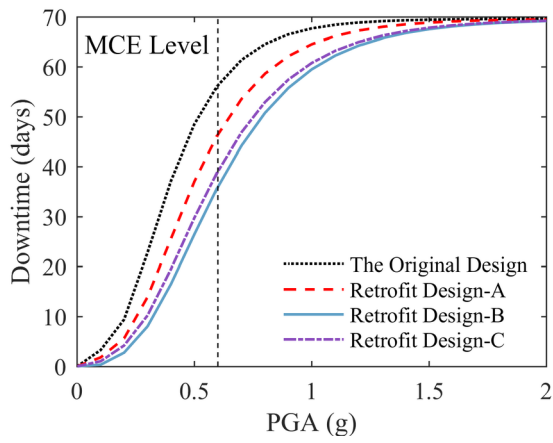
TAL_1719_Figure18.tif

TAL_1719_Figure19.tif

TAL_1719_Figure20.tif

TAL_1719_Figure21.tif

TAL_1719_Figure22.tif

TAL_1719_Figure23.tif